Climate Dynamics

Observational constraints on the tropospheric and near-surface winter signature of the Northern Hemisphere stratospheric polar vortex

--Manuscript Draft--

Manuscript Number:	CLIDY-D-13-00478R3
Full Title:	Observational constraints on the tropospheric and near-surface winter signature of the Northern Hemisphere stratospheric polar vortex
Article Type:	Original Article
Keywords:	stratospheric polar vortex; ENSO; QBO; winter climate; teleconnections; reanalysis; volcanic eruptions
Corresponding Author:	Hans -F. Graf University of Cambridge, Centre for Atmospheric Science Cambridge , UNITED KINGDOM
Corresponding Author Secondary Information:	
Corresponding Author's Institution:	University of Cambridge, Centre for Atmospheric Science
Corresponding Author's Secondary Institution:	
First Author:	Hans -F. Graf
First Author Secondary Information:	
Order of Authors:	Hans -F. Graf
	Davide Zanchettin
	Claudia Timmreck
	Matthias Bittner
Order of Authors Secondary Information:	
Abstract:	A composite analysis of Northern Hemisphere's mid-winter tropospheric anomalies under the conditions of strong and weak stratospheric polar vortex was performed on NCEP/NCAR reanalysis data from 1948 to 2013 considering, as additional grouping criteria, the coincidental states of major seasonally relevant climate phenomena, such as ENSO, QBO and strong volcanic eruptions. The analysis reveals that samples of strong polar vortex nearly exclusively occur during cold ENSO states, while weak polar vortex is observed for both cold and warm ENSO. The strongest tropospheric and near-surface anomalies are found for warm ENSO and weak polar vortex conditions, suggesting that internal tropospheric circulation anomalies related to warm ENSO constructively superpose on dynamical effects from the stratosphere. Additionally, substantial differences are found between the continental winter warming patterns under strong polar vortex conditions in volcanically-disturbed and volcanically-undisturbed winters. However, the small-size samples obtained from the multi-compositing prevent conclusive statements about typical patterns, dominating effects and mechanisms of stratosphere-troposphere interaction on the seasonal time scale based on observational/reanalysis data alone. Hence, our analysis demonstrates that patterns derived from observational/reanalysis series need to be taken with caution as they not always provide sufficiently robust constraints to the inferred mechanisms implicated with stratospheric polar vortex variability and its tropospheric and near-surface signature. Notwithstanding this argument, we propose a limited set of mechanisms that together may explain a relevant part of observed climate variability. These may serve to define future numerical model experiments minimizing the sample biases and, thus, improving process understanding.

Observational constraints on the tropospheric and near-surface winter signature of the Northern Hemisphere stratospheric polar vortex

Hans-F Graf[1*], Davide Zanchettin[2], Claudia Timmreck[2], and Matthias Bittner[2]

[1] *Centre for Atmospheric Science, University of Cambridge, Downing Place, Cambridge CB2 3EN, UK*

[2] *Max Planck Institute for Meteorology, Bundesstr. 53, 20146 Hamburg, Germany*

* corresponding author: hfg21@cam.ac.uk

Abstract

A composite analysis of Northern Hemisphere's mid-winter tropospheric anomalies under the conditions of strong and weak stratospheric polar vortex was performed on NCEP/NCAR reanalysis data from 1948 to 2013 considering, as additional grouping criteria, the coincidental states of major seasonally relevant climate phenomena, such as ENSO, QBO and strong volcanic eruptions. The analysis reveals that samples of strong polar vortex nearly exclusively occur during cold ENSO states, while a weak polar vortex is observed for both cold and warm ENSO. The strongest tropospheric and near-surface anomalies are found for warm ENSO and weak polar vortex conditions, suggesting that internal tropospheric circulation anomalies related to warm ENSO constructively superpose on dynamical effects from the stratosphere. Additionally, substantial differences are found between the continental winter warming patterns under strong polar vortex conditions in volcanically-disturbed and volcanically-undisturbed winters. However, the small-size samples obtained from the multi-compositing prevent conclusive statements about typical patterns, dominating effects and mechanisms of stratosphere-troposphere interaction on the seasonal time scale based on observational/reanalysis data alone. Hence, our analysis demonstrates that patterns derived from observational/reanalysis time series need to be taken with caution as they not always provide sufficiently robust constraints to the inferred mechanisms implicated with stratospheric polar vortex variability and its tropospheric and near-surface signature. Notwithstanding this argument, we propose a limited set of mechanisms that together may explain a relevant part of observed climate variability. These may serve to define future numerical model experiments minimizing the sample biases and, thus, improving process understanding.

1. Introduction

For about two decades there has been growing evidence in observational and model studies that tropospheric circulation and regional climates in boreal winter can be modulated by the strength of the Northern Hemisphere (NH) stratospheric polar vortex (e.g., Baldwin et al., 1994; Perlwitz and Graf, 1995; Kodera et al., 1996). The general picture suggests at least some degree of linearity in the tropospheric and near-surface signatures of the polar vortex,

so that continental winter cooling corresponds to weak polar vortex conditions (e.g., Baldwin and Dunkerton, 2001) while continental winter warming corresponds to strong polar vortex conditions (e.g., Graf et al., 1994). A number of mechanisms have been proposed based on observational and simulated data to explain the linkage between stratospheric polar vortex and tropospheric circulation, but there is still lack of theoretical understanding and numerical models and observations often disagree (for an extensive discussion see Gerber et al., 2012). It remains unclear how much the dominant processes (and forcing agents) behind mechanisms of stratosphere-troposphere interactions themselves directly impact the tropospheric circulation and thereby alter the polar vortex's signature on surface regional climates. In this study, we perform such an assessment based on observational/reanalysis data and focusing on the seasonal time scale and on a few major features of interannual climate variability.

Since the earliest studies on the mechanisms of stratosphere-troposphere/surface interaction, investigations of the volcanically-forced atmospheric dynamics greatly raised interest and stimulated the debate on this topic. Particularly the link of the observed post-eruption strengthening of the polar vortex with the post-eruption enhanced positive phase of the North Atlantic Oscillation (NAO) and continental winter warming (e.g., Graf et al., 1994) stimulated research. This resulted in the scientific literature delineating today a rather varied list of externally-forced and -unforced coupling processes that can be relevant for the observed variability. For instance, reflective properties of strong lower stratospheric winds modulate phase and amplitude of tropospheric Rossby waves (Perlwitz and Graf, 1995; Wittmann et al., 2004), providing an internal mechanism of stratosphere-troposphere interaction. This, however, may be not the dominant coupling process after strong tropical volcanic eruptions (Graf et al., 2007). Perlwitz and Harnik (2004) noted the importance of downward reflection of planetary waves from higher stratospheric levels. Ambaum and Hoskins (2002) mentioned the importance of the modulation of the height of the polar tropopause in response to stratospheric warming or cooling, which leads to positive (negative) polar tropospheric pressure anomalies under weak and warm (strong and cold) stratospheric polar vortex. Castanheira et al. (2009) indicated that the effect of downward propagating zonal wind anomalies in high mid-latitudes and their interaction with topography leads to the typical NAO-type anomaly in the mid-latitude troposphere, while in

agreement with Ambaum and Hoskins (2002) pressure anomalies over the polar cap are due to barotropic effects. The interaction of tropospheric baroclinic eddies with downward propagating wind anomalies at the edge of the polar vortex (Wittmann et al., 2007; Scaife et al., 2012; see also the discussion in Gerber et al., 2012) seems to be an important factor of amplification of initial disturbances in both simple and complex models. This was also shown by reanalysis data for strong and weak polar vortex episodes in terms of Eady growth rates (Walter and Graf, 2005; for a discussion of the underlying mechanisms see Walter and Graf (2006)). It is therefore plausible that different mechanisms are at work at polar and mid-latitudes of the Northern Hemisphere.

Analysis of state-of-the-art coupled climate model simulations shows a large spread in the simulated stratospheric polar response to climate change (e.g. Morgenstern et al., 2010). It also highlights the difficulties to accurately simulate the observed NH winter response after large volcanic eruptions (Driscoll et al., 2012; Charlton-Perez et al., 2013). These difficulties might be due to noise affecting the small sample of observations, but Stenchikov et al. (2006) showed clear dynamic model deficiencies related to the coupling between NAO and polar vortex strength, which have not been fully overcome in later model generations. So, the interpretation of stratosphere-troposphere coupling processes based on current coupled climate model simulations still suffers from non-negligible limitations. Hence, we have to rely on the available reanalysis data as the best source of physically-consistent information about the real atmosphere, but the available length of these data limits the power of statistical analysis and bears the danger of sampling biases. In fact, physical processes involved in climate variability are often inferred from specific properties of the derived patterns. In this case, the question is therefore whether average patterns obtained from observational/reanalysis series provide sufficiently robust constraints to the inferred mechanisms implicated with stratospheric polar vortex variability and its tropospheric and near-surface signatures.

Additional issues for the dynamical interpretation of the observed variability may arise from the diverse temporal scales characterizing the interacting processes. Many of the aforementioned studies focused on individual events of strong and weak polar vortex responsible for intra-seasonal variability. However, changes in the strength of the polar vortex are induced by anomalies of vertically propagating planetary wave activity at time

scales of few days, and the anomalies then last in the stratosphere for much longer (e.g., Castanheira et al., 2009) due to the slow relaxation of the stratosphere by radiative processes. The possibility that the polar vortex anomalies were themselves produced by waves generated in the troposphere was acknowledged in most studies (e.g., Polvani and Waugh, 2004; Gerber and Polvani, 2009). Garfinkel et al. (2013) recently demonstrated using a dry model that in equilibrated simulations the tropospheric internal variability dominates the response of the extra-tropical troposphere to a stratospheric polar vortex, so that the evidence supporting any stratosphere-troposphere coupled mechanism is likely buried under the massive tropospheric variability. Previous studies on stratosphere-troposphere interactions, however, often ignored that the processes and forcing agents responsible for anomalous tropospheric wave activity can themselves persist over longer periods of time and hence can sustainably impact the tropospheric circulation. This might lead to misinterpretation of the imprint of certain established stratospheric polar vortex conditions on observed tropospheric anomalies, and hence of related mechanisms, especially since the dataset is short and, thus, prone to sampling biases. Such anomalies, which are persistent for more than a season and which we concentrate on include those of volcanic origin, El Niños/La Niñas (or warm/cold states of the El Niño-Southern Oscillation or ENSO), the Quasi Biennial Oscillation (QBO) and, potentially, variations in the solar irradiance. Other such features, which will not be covered within the current study, are early Siberian snowfall (Cohen et al. 2007), as well as North Pacific and Indian Ocean sea-surface temperatures (Hurwitz et al., 2012; Fletcher and Kushner, 2011) and decadal variability of North Atlantic temperatures (Schimanke et al., 2011).

The strong variability of tropical Pacific sea-surface temperature anomalies (SSTAs) related to the ENSO phenomenon cause variability in deep tropical convection and in generation of Rossby waves. This is particularly critical due to its global tropospheric teleconnections and its influence on stratospheric dynamics (e.g., Ineson and Scaife, 2009). Early suggestions of El Niño leading to weak polar vortex are from van Loon and Labitzke (1987). Garfinkel and Hartmann (2007) as well as Wei et al. (2007) were able to show that the cold phase of ENSO typically leads to strong vortex in the polar stratosphere. In addition, Taguchi and Hartmann (2005) demonstrated that the tropospheric anomaly patterns over the Pacific/North American sector observed at sudden stratospheric warmings (episodes of very weak polar

vortex) depend on the state of ENSO. Using a high-top climate model forced by observed SSTAs, Manzini et al. (2006) showed that El Niños can weaken the stratospheric polar vortex with subsequent impact on the troposphere via the zonal-mean flow, but they did not find any significant effect of La Niñas. Moreover, ENSO patterns have changed during the last decades, with Central Pacific and hybrid El Niños recently becoming more frequent (Johnson, 2013). Such a change in SSTA patterns and, consequently, also in latent heating of the tropical troposphere may have impacted the strength and shape of global teleconnections (Kodera, 2010; Graf and Zanchettin, 2012; Garfinkel et al., 2012). Kodera (2010) suggests that changes in El Niño patterns lead to changes in its teleconnectivity, with El Niños prior to 1978 mainly affecting the strength of the polar vortex via the Pacific-North American pattern (PNA), while mainly leading to a strengthened subtropical jet afterwards. However, the same change of teleconnections may as well have been induced by the changes of the location where tropical Pacific SSTAs induce deep convection and latent heat release (Jin and Hoskins, 1995; Graf and Zanchettin, 2012). Of course, in its different definitions ENSO expresses only part of the tropical Pacific climate variability. For instance, since the end of the 20th century strong warming of the tropical sea surface not related to the ENSO phenomenon extended from the Indian Ocean to the Western Pacific. Since this warming influences deep tropical convection and latent heat release over the Western Pacific as well, it is potentially influencing or modulating the contribution of tropical Pacific anomalies to Atlantic and European seasonal climate anomalies (Walter and Graf, 2002).

Garfinkel and Hartmann (2007, 2008) demonstrated that during La Niña conditions, independent of the phase of the QBO, the wave number one disturbance in high northern mid-latitudes is in quadrature with its climatological pattern and resembles a negative phase of the PNA, hence supporting the development of a strong polar vortex. This result is in contradiction to the simulations by Manzini et al. (2006), who did not find a significant effect of La Niñas on the stratosphere. Under El Niño conditions, now in line with Manzini et al.'s (2006) study, the Aleutian Low is enhanced and a positive phase of the PNA is prominent, leading to stronger wave activity flux into the stratosphere and a weak polar vortex. This effect is stronger for westerly than for easterly QBO. Different pathways are described for the ENSO signal to reach Eurasia, which include a subtropical (Jin and Hoskins, 1995;

Branstator, 2002) and a mid-latitude tropospheric wave train as well as the stratosphere-troposphere coupling (Brönniman, 2007; Cagnazzo and Manzini, 2009).

Overall, the multiplicity - and in some aspects incongruence - of the above-mentioned mechanisms points to our inability to fully disentangle the complexity of the climate system especially due to the limitations inherent in the two available tools: incompleteness of simulated processes and exiguity of observations. On the other hand, in the current situation of a relatively short observational time series it is of essential importance to identify biased observational features and accordingly re-review proposed mechanisms, i.e. our current understanding of observed climate dynamics. In this study we concentrate on features of seasonal and lower frequency climate variability that dynamically interact with the stratospheric polar vortex, especially as precursors in its development phase, and that persist long enough to imprint themselves on tropospheric and near-surface patterns, thereby influencing the tropospheric signature of the stratospheric polar vortex in its established phase. Among these features are tropical Pacific SSTAs, the QBO phase as well as solar irradiance and strong volcanic eruptions. It is interesting to investigate with these features in mind:

- To what degree are the tropospheric anomaly patterns linearly related to the strength of the stratospheric polar vortex?
- Are there sampling biases invoked by tropospheric mechanisms favouring strong or weak vortices in the stratosphere?
- To what degree can we distinguish between effects of the polar vortex and other linked or coinciding features?

We will first briefly introduce the data and methodology used. We will then show how ENSO, QBO and solar activity phases are aligned to strong and weak polar vortex winters. Anomalies related to volcanic eruptions are discussed separately. Composite analysis will provide information about asymmetries in the climate anomalies of near-surface temperature and mid-tropospheric pressure fields during strong and weak polar vortex winters. The anomalous patterns will serve, supported from analysis on additional climate parameters as appropriate, as basis to critically discuss formerly proposed mechanisms and

dominant processes behind the connection between polar vortex and tropospheric weather and climate. We will concentrate on the main winter months - January and February - since then the strongest anomalies can be expected, unaffected by the build-up and dissolution processes of the polar vortex. We therefore focus on the low-frequency processes in NH winter associated to an already established background state described by certain persisting polar vortex conditions and coincident persisting tropospheric anomalies.

2. Data and methods

We use monthly-mean data of geopotential height at 500 hPa and 50 hPa levels, near-surface (1000 hPa) air temperature, sea-surface temperature and precipitation rate at the surface obtained from NCEP reanalysis (Kalnay et al., 1996) for the period 1948/01 until 2013/04. The data were provided by the NOAA/OAR/ESRL PSD, Boulder, Colorado, USA. NCEP/NCAR reanalysis data are widely used for inferences about different aspects of the Earth system's dynamics and variability and have proven to be a reliable source of information especially for large-scale process analysis. The analysis is conducted on mid-winter (January-February, or JF) average time series covering the period 1948-2013. Local linear trends were removed before the analysis. If not mentioned otherwise we exclude from our analysis all winters that were impacted by the three big volcanic eruptions of Agung (February 1963, winters 1963/64 and 1964/65), El Chichón (March 1982, winters 1982/83 and 1983/84) and Pinatubo (June 1991, winters 1991/92 and 1992/93). Anomalies are calculated as seasonal deviations from the local seasonal climatology. Significance of the anomalies is assessed based on random occurrence (500 surrogate data sets) as in Graf and Zanchettin (2012). The same randomization approach is followed to assess the significance of differences between selected composite patterns. In all figures statistically non-significant ($p>0.05$) local statistics are indicated by dots.

Since we are interested in the signature of the stratospheric polar vortex on tropospheric climate, our results are based mainly on a composite analysis for the strongest and weakest of polar vortices during the investigated period. The strength of the stratospheric polar vortex is calculated via the JF mean geopotential height anomaly at the 50 hPa level over the northern polar cap (north of 65^{o}N). A Polar Vortex Index (PVI) is accordingly defined as the

inverted and linearly detrended standardized time series of the so-defined geopotential height data (Figure 1a). Winters characterized by strong and weak polar vortex correspond to those years when PVI is, respectively, above 1 and below -1. Selected years with strong polar vortex are 1967, 1972, 1974, 1976, 1989, 1990, 1996, 1997, 2000, and 2005. Selected years with weak polar vortex are 1958, 1960, 1970, 1977, 1985, 1987, 2004, 2006, 2009, 2010 and 2013. Four of the six volcanically-affected winters were also characterized by strong polar vortices (1964, 1983, 1984, and 1993); these are analysed separately. We note that previous to 1957 there were no strong PVI anomalies detected in the NCEP reanalysis, which may be due to incomplete information available on the stratosphere before the International Geophysical Year 1957.

We also make use of the following indices. The December-January Niño3.4-index anomalies from the 30-year climatology (www.cpc.ncep.noaa.gov/products/analysis_monitoring/ensostuff/ detrend.nino34.ascii.txt), as used to calculate the Oceanic Niño Index (ONI) index, are used to identify winters characterized by warm (index ≥ 0.5) and cold (index ≤ -0.5) ENSO conditions (Figure 1b). The so-defined ENSO index allows accounting for the time needed by wave disturbances from the tropics to propagate into higher latitudes and the stratosphere. Using a JF ENSO would change the sampling of coupled ENSO and PVI states for warm ENSO/strong PVI (empty bin), warm ENSO/weak PVI (by exclusion of winter 1969/70) and cold ENSO/strong PVI (by exclusion of winters 1971/72 and 1996/97). The QBO index (www.esrl.noaa.gov/psd/data/correlation/qbo.data) is used to determine the QBO phase in early winter. QBO is marked “west” if the 30 hPa zonal mean wind at the equator is exceeding 4 m/s and “east” if it is less than -4 m/s. Slightly increasing these limits has no effect on the grouping. The November monthly-mean value of the QBO index is considered to take into account the ~45 day relaxation time of the stratosphere. Using the JF or DJ QBO only marginally changes the grouping results. Solar irradiance described by the solar 10.7 cm index obtained from www.spaceweather.ca/data-donnee/sol_flux/sx-6-mavg-eng.php was defined as low or high irradiance when the index is below 125 and above 140, respectively (Camp and Tung, 2007).

3. Results

Figure 2 illustrates some conventional linear regression results between the strength of the polar vortex (Figure 1a) and selected NH atmospheric climate parameters based on reanalysis winter data for the full 1948-2013 period. Linear analysis shows that the polar vortex extensively imprints on stratospheric (Figure 2a) and mid-tropospheric (Figure 2b) circulation as well as on near-surface regional temperatures (Figure 2c). For a strong polar vortex the NAO is in its positive phase, mid- and high latitudes over Eurasia are anomalously warm, and Northeast Canada and especially the Davis Strait are anomalously cold. Negative temperature anomalies also appear over North Africa, the Middle East and southern Central Asia. This is in agreement with results from the early 1990s (e.g., Perlwitz and Graf, 1995) and this relationship was indeed used to explain, for instance, continental winter warming after strong tropical volcanic eruptions (Graf et al., 1993; Robock, 2000). SSTAs point towards colder conditions in the tropical Pacific under strong polar vortex, but the regressions are weak and only locally significant (Figure 2d). When the six volcanically impacted winters are excluded, the linear regression patterns remain qualitatively unchanged, but the statistical significance of near-surface temperature anomalies (Figure 2 e-g) is strongly reduced especially over Eurasia, while the cold signal in tropical Pacific SSTAs becomes more prominent (Figure 2h). Linear regression implicitly assumes that the underlying processes responsible for the statistical relationship are symmetric, i.e. the tropospheric signature of weak polar vortex conditions entails the same spatial patterns as that of strong polar vortex conditions but with opposite sign, e.g., a weak polar vortex leads to anomalously cold conditions over mid- and high-latitude Eurasia (compare Figure 2c). Given the rather small number of years that can be used to perform such statistical analysis and given that a variety of potential mechanisms of stratospheric impact on the troposphere have been proposed, it is worthwhile to investigate if “linearity” really is a suitable principle. In particular, as recent simulations by Fletcher and Kushner (2011) show, decreasing the strength of the climatological stationary wave reduces the importance of linear interference between the SSTAs in the tropical Pacific and the northern annular mode, and increases the importance of nonlinearity. This simulated extra-tropical annular mode response to climate forcings is found to be quite sensitive to the amplitude and phase of the climatological stationary wave and the wave response.

The assumption of symmetric tropospheric signatures of anomalously strong and weak polar vortex conditions can be tested by simple composite analysis for a number of very strong versus a number of very weak polar vortices (defined by PVI exceeding +/- one standard deviation). If the two composites sample from anomalous polar vortex conditions of similar amplitude and in the case of strong symmetry, the sum of the two composites should become evanishing small. Conversely, if substantial asymmetry occurs in any direction, included a biased sampling, local differences significantly different from zero must appear. Following our definition, the anomalously strong and weak polar vortex conditions account for composite PVI values of 1.351±0.272 and -1.542±0.246 (mean ± standard deviation), respectively. The selected weak polar vortex conditions are therefore, on average, slightly more intense than the strong polar vortex ones. Nonetheless, in their absolute values, the two groups are not significantly different according to a Mann-Whitney U test ($p>0.05$ for a two-tailed test). Linearity in the associated patterns is inferred by using composite analysis according to the criterion $|PVI|\geq 1$. In general, evanishing anomalies indicate that there is symmetric behaviour in the troposphere within the given limits of statistical significance despite a possible bias towards weak polar vortex conditions (not shown). The above discussed results are derived from rather small ensembles, and the results, hence our inference of overall linearity, may be affected by spurious statistics due to the limited sampling. As mentioned above, a number of factors with characteristic timescale of at least one season might influence the results: ENSO, QBO, and solar activity. The volcanically impacted winters were excluded from the analysis and will be discussed separately.

The matrix in Table 1 illustrates how the weak and strong polar vortex winter composites are aligned with the states of the DJ ENSO, of the November QBO phase and of solar activity. There is indeed some potential sampling problem if one looks solely from the point of stratosphere-troposphere coupling as most (7 out of 10) strong polar vortices occurred during cold ENSO. Hence, the observed anomalies in the troposphere will be a combination of tropospheric teleconnection to La Niña plus a potential impact from the stratosphere. There is only one strong PVI event under warm ENSO (2005), when the polar vortex was strongly displaced from the pole and had its centre over the Canadian Arctic (not shown). Using the JF ENSO index would remove this winter from the warm ENSO/strong PV bin. It would deserve a specific investigation, which is beyond the scope of the current study and

will be ignored in the following discussion. In 1967 the ENSO index is negative, but not exceeding -0.5 standard deviations, so being regarded as near neutral. The 1990 ENSO index is near zero, hence clearly neutral.

In accordance with previous findings, most of the strong polar vortex winters follow a westerly (6 out of 10) or neutral (2 out of 10) phase of the QBO. The only exceptions are the winters of 1990 and 1997, which were preceded by an easterly QBO in November. Cold ENSO and westerly QBO conditions are favourable for reduced wave activity flux into the stratosphere: Less tropical Rossby wave activity is generated due to reduced precipitation in the tropical Pacific, tropical waves are reflected back towards the equator and the Aleutian Low is weak (see, e.g., Garfinkel and Hartmann, 2010). Six of the ten strong polar vortex winters occurred during weak solar irradiance, four of them during strong solar irradiance. This does not indicate a preferred link of a strong polar vortex with solar irradiance. Hence, we will not consider solar irradiance in the following discussion. In any case the result supports the statement of Camp and Tung (2007) that there is “a least disturbed situation of the stratospheric polar vortex (the vortex is cold and strong) when ENSO is in its cold phase, QBO is west and solar activity is low”. Weak polar vortex is found for both, cold and warm ENSO with the easterly QBO slightly dominating, but again solar irradiance is quite equally distributed. Having weak polar vortex in both ENSO phases is in agreement with Butler and Polvani (2011), who demonstrated equal probability of sudden stratospheric warming for cold and warm ENSO. ENSO is obviously not the only phenomenon that can disturb the formation of the polar vortex.

In summary, our sample is clearly dominated by cold ENSO conditions during strong polar vortex winters. However, the occurrence of cold ENSO conditions does not necessarily correspond to strong stratospheric polar vortex as, similarly, not all warm ENSO winters are accompanied by weak polar vortex. This allows inferring, through comparison of composite anomalous patterns, the relative importance of contributions from tropospheric processes linked to the state of ENSO for the tropospheric signature of strong and weak polar vortex conditions. This is explored in the next sections. We will first take on the perspective of a season’s forecaster by looking at significant anomalies during different constellations of ENSO and polar vortex. This is followed by analysis of the differences between composite pairs aimed at further clarifying the individual effects of polar vortex, ENSO and volcanic

forcing. Due to their different construction, we only qualitatively compare the regression patterns (Figure 2) and composite patterns (Figures 3, 4, 6, 8).

3.1 Polar vortex and ENSO

A composite analysis is performed on the reanalysis field data based on Table 1, using PVI as grouping criterion, and ENSO as pre-grouping criterion. Specifically, we concentrate on a comparison of mid-winter anomalies of strong and weak polar vortex during warm and cold ENSO states (i.e., exceeding ±0.5 standard deviations). Figure 3 illustrates the anomalous patterns associated to the seven winters characterized by *strong polar vortex and cold ENSO* conditions. The deepening of 50 hPa geopotential heights indicates the stronger-than-average stratospheric polar vortex (Figure 3a). The significant negative SSTAs in the Central Pacific, the Indian Ocean and the Caribbean Sea reflect the sampled cold ENSO state (Figure 3d). They do not represent a typical La Niña pattern, which would entail large and extensively significant Eastern Pacific SSTAs, but rather a Central Pacific La Niña pattern (Johnson, 2013). The mid-tropospheric pressure anomalies (Figure 3b) only partly project on the NAO in the central North Atlantic as would have been expected from linear regression analysis (Figure 2), specifically since the southern belt of high pressure anomaly is separated into two distinct centres. Temperature anomalies in the lower troposphere (Figure 3c) can be explained by the anomalous advection of air masses associated to the anomalous atmospheric circulation pattern (Figure 3b). They grossly overlap with the linear regression pattern in Figure 2c, but distinguishing traits are found as well. Most importantly, the warming pattern over Eurasia expected from linear regression analysis is missing. There is just a local positive temperature anomaly over Scandinavia to the north of the mid-tropospheric high pressure anomaly suggesting its origin as warm air advection from the Atlantic sector likely due to increased blocking activity over Europe. Negative temperature anomalies along the North Pacific coast can be linked to the weakened, though not significantly, Aleutian Low. As seen in the linear regression pattern (Figure 2c), the temperature anomaly dipole over the eastern parts of North America is typical for circulation anomalies evolving from the pressure anomaly dipole over the western North Atlantic with low pressure to the north and high pressure to the south. Similarly, the strong cold anomalies in eastern North Africa and the Middle East are likely produced by advection

388 of cold continental air between the European high pressure and the low pressure anomaly
389 over Middle Asia.

390 Figure 4 illustrates the anomalous patterns associated to the four winters characterized by
391 *weak polar vortex and cold ENSO* conditions. Positive pressure anomalies in the lower
392 stratosphere reflect the weaker-than-normal polar vortex; they are centred over the pole
393 with some extension towards Greenland and Northern Eurasia (Figure 4a). In the ENSO
394 region, SSTAs are overall negative, but only locally significant (Figure 4d). Again, tropospheric
395 anomalies only partially overlap with the linear regression pattern in Figure 2c. Pressure
396 anomalies in the mid-troposphere (Figure 4b) prominently differ from the pattern expected
397 from linear regression: significant centres emerge over the eastern North Pacific (in line with
398 the expected response of the Aleutian Low to the cold tropical Pacific SSTAs), over the
399 Greenland, Iceland and Norwegian Seas (positive) and over Central Europe and the
400 Mediterranean (negative). Hence, the hemispheric signature does not resemble the negative
401 NAO-like pattern over the Atlantic as expected from linear regression on PVI (Figure 2b).
402 Temperature anomalies in the lower troposphere are generally rather weak and only locally
403 significant (Figure 4c). Nonetheless, consistent with the gross features of the pattern
404 expected from linear regression, anomalies over Eurasia are negative in a large belt across
405 the mid-latitudes associated with a warm belt at its southern flank.

406 Figure 5 demonstrates that there are statistically significant differences between the
407 tropospheric patterns associated with weak and strong polar vortex conditions under similar
408 cold ENSO conditions. Tropical Pacific SSTs only sporadically exhibit significant differences
409 (Figure 5d); significant differences between tropospheric geopotential heights concentrate
410 on the North Atlantic and Eurasia with a clear barotropic effect over the Canadian Arctic and
411 the Greenland, Iceland and Norwegian Seas (Figure 5b). In the midlatitudes there is some
412 indication of a circum-global zonal wave train along approximately 45-50^{o} N. Near-surface
413 temperature differences show a warmer Arctic at weak polar vortex especially over the
414 Labrador Sea and surrounding regions (Figure 5c). Over Eurasia significant differences occur
415 only over Central and Northern Europe (colder during weak polar vortex), while same-sign
416 differences over the Far East of Siberia and Central China are much weaker. There is a strong
417 and significant belt of positive temperature differences (weak minus strong polar vortex)

418 extending from Northeast Africa across the Middle East to Northern India and West China,
419 which also imprints on the mid-tropospheric geopotential height.

420 Figure 6 shows the anomalous patterns associated to the five winters characterized by *weak*
421 *polar vortex and warm ENSO* conditions. The anomalous 50 hPa geopotentential height
422 pattern (Figure 6a) indicates that the weak stratospheric polar vortex does not extend as
423 strongly over Scandinavia and Northern Siberia as for the cold ENSO conditions (compare
424 Figure 4a). It also entails a quasi-circumpolar belt of low pressure anomalies in the mid-
425 latitudes, significant over the Eastern Hemisphere. This pressure anomaly pattern points
426 towards reduced zonal winds along the edge of the stratospheric polar vortex. The positive
427 tropical Pacific SSTAs indicate Central Pacific warming (Figure 6d). This is consistent with
428 Garfinkel et al. (2012) but not with Hegyi and Deng (2011). Again, the NH anomalous
429 patterns in the mid- and lower troposphere only partially overlap with the linear regression
430 pattern in Figure 2c. They also substantially differ regionally from those in Figure 4,
431 especially over the North Pacific and North America, as a consequence of the sampled
432 warmer state of ENSO (Figure 7d). In accordance with the tropical Pacific SSTAs and
433 associated locally enhanced precipitation rates (not shown), a strongly enhanced low
434 pressure anomaly is established over the North Pacific (Figure 6b) corresponding to a
435 strengthened Aleutian Low. From the southern United States and Mexico across the North
436 Atlantic and well into Western Europe a belt of highly significant low pressure anomalies is a
437 very prominent feature of the mid-tropospheric geopotential height anomaly pattern. The
438 strongest positive mid-tropospheric geopotential height anomaly appears over South
439 Greenland and the Davis Strait. This anomaly covers also large parts of Canada and the
440 North Pole, and it extends to the east towards Iceland, Spitsbergen and the Russian Arctic.
441 The high latitude positive and the mid-latitude negative geopotential height anomalies
442 clearly project on a strong negative phase of the NAO.

443 Cold near-surface temperature anomalies dominate northern Eurasia with centres over
444 North and East Europe and central Siberia (Figure 6c), in good accordance with expectations
445 during a negative phase of the NAO, and are indeed quite similar to the anomalies for weak
446 polar vortex and cold ENSO conditions (Figure 4c). In this case, however, the negative
447 anomaly over Europe is located over Scandinavia, whereas under cold ENSO conditions it
448 was displaced over the continent. The strength and extent of temperature anomalies over

North America are the most distinguishing features of this composite pattern: they reflect the configuration of hemispheric-scale circulation described by a coupled positive PNA/negative NAO state (compare with, e.g., Zanchettin et al., 2012).

The differences between warm and cold ENSO phases at weak polar vortex (Figure 7) indicate a shift of the polar vortex towards the Eastern Hemisphere at warm ENSO resulting in a positive (negative) height anomaly at 50 hPa over western North America (North Atlantic and North Europe). A similar shift was also reported based on surface pressure observations (Quadrelli and Wallace, 2002). Differences between the mid-tropospheric geopotential patterns include a strongly enhanced Aleutian Low during warm ENSO with the associated typical positive PNA pattern. The low pressure anomaly over the Nordic Seas and Northern Europe is a barotropic effect of the polar vortex displacement. Near-surface temperature differences are significant mainly over North America (Figure 7c) as an effect of circulation anomalies linked to the positive PNA pattern at warm ENSO.

In summary, our composite analysis reveals that the state of ENSO significantly interferes with the tropospheric and near-surface signatures of the polar vortex, particularly concerning the North Pacific/North American/western North Atlantic sector. The polar vortex's signature over Eurasia is overall consistent with the expectation from linear regression, with generally colder conditions under weak vortex, and vice versa. Nonetheless, regional details of this response are likely to be affected by ENSO also in this region, especially in terms of geopotential height over the Nordic Seas and Scandinavia. These geopotential height anomalies do not manifest themselves in temperature anomalies, which, for the data available, seem to be dominated over Eurasia by the polar vortex.

3.2 Volcanic effects

There is evidence that strong stratospheric polar vortices have developed after the strongest tropical volcanic eruptions, which we have excluded from the previous analyses. Under volcanically-forced conditions the gradient of radiative heating at the stratospheric aerosols between lower and polar latitudes leads to a forcing of the polar vortex already during its developing phase in fall. This in turn leads to enhanced lower stratospheric westerlies that prevent wave activity flux entering stratospheric heights and thereafter penetrate down into the subpolar troposphere. For strong aerosol loadings this heating gradient may override the

counter-acting effects from tropospheric wave disturbances of the vortex. In case of volcanic impact the stratospheric polar vortex is directly radiatively forced in-situ. This is different from the cases presented above, for which the strong polar vortex evolved due to lack of planetary wave disturbances. The four volcanic winters with strong stratospheric polar vortex were characterized by diverse states of ENSO (Figure 1b). It is therefore relevant to compare anomalous patterns associated to strong polar vortex conditions in volcanically-disturbed winters (Figure 8) and in volcanically-undisturbed winters (Figure 3).

Anomalous 50 hPa geopotential heights indicate a strong polar-symmetric stratospheric vortex (Figure 8a) in volcanically disturbed winters. The positive anomalies at tropical and sub-tropical latitudes reflect the radiative effects of volcanic aerosols. The enhanced meridional geopotential gradient in subpolar latitudes produces enhanced zonal winds which will penetrate into the troposphere and interact with the topography. Overall there are close similarities with Figure 3a although the polar vortex is more compact, leading to enhanced westerlies at the edge of the vortex at latitudes close to the polar circle. There are also major differences in the oceanic boundary conditions as strong polar vortex in non-volcanic winters nearly exclusively occurred during cold ENSO conditions (Figure 3d), while average tropical Pacific SSTAs during the volcanic winters are positive especially in the eastern region (Figure 8d). We do not further discuss the co-occurrence of warm ENSO and strong tropical volcanic eruptions, but note that a recent paleoclimate record points toward a multi-centennial robust link between major volcanic events and El Niño-like anomalous warming in the tropical Pacific (Li et al., 2013). The most striking difference between Figures 3 and 8 is that the strong near-surface warming over Siberia during volcanic winters (Figure 8c) is missing in non-volcanic winters with similarly strong polar vortex in the stratosphere (Figure 3c) and is replaced by a tendency towards negative temperature anomalies. Accordingly, during volcanic winters, the mid-tropospheric pressure anomalies (Figure 8b) are characterized by a high pressure centre over the eastern mid-latitude North Atlantic and Western Europe, and a low pressure centre over the Labrador Sea/Davis Strait. In contrast, during non-volcano winters the mid-tropospheric pressure anomalies are dominated by the West Atlantic dipole, with a weaker high pressure anomaly over Europe (Figure 3b). Both patterns partly project on a positive NAO pattern, and the different locations of the

anomalous centres seem not sufficient to explain the differences in temperature anomalies over the more continental Eurasia.

To verify that average winter climates characterized by strong polar vortex under volcanically-forced and undisturbed conditions are significantly different we perform a randomization-based test. Figure 9 summarizes these differences. Of course, there are massive differences in SSTAs both in the Pacific and Indian Oceans, since volcanic winters sample much warmer tropical SSTAs (Figure 8d) whereas only cold ENSO conditions allowed a strong polar vortex to develop under undisturbed conditions (Table 1). Hence, there is also a strong difference in the intensity of the Aleutian Low, which is much deeper in the volcanic winters (Figure 9b). On the one hand, the prominence of the SST and SST-related differences complicates our interpretation of tropospheric anomalies at the hemispheric scale. On the other hand, barotropic phenomena dominate the tropospheric behavior in the polar regions under strong volcanic forcing (Figure 8a,b). This effect largely explains the differences in the mid-tropospheric patterns (Figure 9b) and associated continental warming over North America and over Siberia (Figure 9c). In contrast, the higher pressure over the eastern North Atlantic in volcanic winters compared to undisturbed cold ENSO conditions clearly exhibits a baroclinic character with a tendency towards lower temperatures at the surface and no imprint on the stratospheric geopotential height (Figure 9a-c). This suggests that the differences arise mostly due to different tropospheric, possibly ENSO-related conditions.

Figure 10 compares the anomalies of the 850 hPa zonal wind during strong polar vortex winters under volcanically-undisturbed (panel a) and volcanically-disturbed (panel b) winters. In volcanic winters a strong and rather narrow band of circumpolar enhanced zonal winds is found along the polar circle, while zonal winds are enhanced in a more patchy way and shifted towards North America in non-volcanic winters. Significant differences with enhanced westwind over the high latitude North Atlantic and over northern Siberia and with reduced zonal wind in the case of volcanic winters over the eastern United States may in part explain the differences in near-surface temperature. The related advective anomalies and the interaction of these anomalous winds with topography (see Castanheira et al. 2009, who, different from Figure 10 looked at the barotropic component of zonal wind) provide an additional plausible explanation for the differences in near-surface Eurasian temperatures.

4. Discussion

From the above results it seems clear that, with the exception of volcanically disturbed winters, in accordance with Garfinkel and Hartmann (2007) the strongest polar vortices evolved under the favourable conditions of cold ENSO supported by westerly QBO. These conditions will have had an impact on the evolution of tropospheric climate anomalies and it is important to disentangle the effects of strong stratospheric vortex from those related to cold ENSO and westerly QBO. While model simulations forced towards strong polar vortex in the stratosphere (e.g., Scaife et al., 2005) have provided evidence that a strong stratospheric polar vortex can result in a positive NAO and warm near-surface temperature anomalies over Eurasia, in the reanalysis data used here these features cannot be detected with similar significance. Only for the volcanic winters do we see comparable anomalies. Beside sampling-related issues, this is quite possibly due to the accompanying conditions for strong polar vortex evolution. These conditions originate and persist in the troposphere where they strongly impact the tropospheric anomalies in addition to the mechanisms originating from the stratospheric anomalies. One important question is therefore whether the formation of a very strong NH stratospheric polar vortex is limited to cold ENSO conditions in an otherwise unperturbed coupled ocean-atmosphere system. In their temporally limited coverage, reanalysis data confirm a strong supportive function of cold ENSO for the evolution of strong polar vortex in the stratosphere. It is, however, expected that different sources of planetary wave activity in the NH higher latitudes may contribute in those cases when a weak polar vortex develops during cold, but also neutral, ENSO conditions. For instance, early winter positive snow cover anomalies in West Siberia (e.g. Cohen et al., 2007) are a candidate. Butler and Polvani (2011) showed that sudden stratospheric warmings (SSW) are equally frequent in warm and cold ENSO states. ENSO is not the only important factor for the evolution of anomalous polar vortices. However, as also clearly shown here, processes that lead to variability of the stratospheric polar vortex also have the potential to directly impact tropospheric variability.

The comparison of winter anomalies under weak polar vortex, but with different ENSO states indicates that ENSO's phase plays a significant role mainly for the Pacific North American and

Western Atlantic sector. At cold ENSO the significant differences between strong and weak polar vortex are concentrated on the North Atlantic and the Eurasian continent. For strong vortex we cannot make any statement on ENSO effects since a warm case only occurred once. However, there are differences in those winters with strong vortex that originated from the lack of wave disturbance (non-volcanic) or were driven by radiative forcing in the stratosphere (volcanic). In the first case PNA is negative and imprints on both the troposphere and the stratosphere. In the second case forcing is in-situ in the stratosphere, is zonally symmetric and very strong. In this case, tropospheric anomalies are due to interaction of downward penetrating zonal wind anomalies and barotropic effects resulting from the shift of the polar vortex into a polar symmetric position.

In the following we will discuss possible relevant mechanisms inferred from the anomalous patterns derived from the reanalysis data, after a brief reflection on the specific case of a volcanically-disturbed system. Our discussion aims to clarify how the limited length of the observational data series together with the dominance of internal tropospheric variability on stratosphere-troposphere coupled processes (Garfinkel et al., 2013) prevents an unambiguous discrimination of the processes dominating seasonal variability in the winter troposphere based on reanalysis data alone.

In volcanically-disturbed winters the stratospheric polar vortex is forced in-situ by the large meridional temperature gradient caused by radiative processes involving the volcanic aerosols (e.g., Zanchettin et al., 2012). This process is basically polar symmetric and the heating gradient may override the counter-acting effects from tropospheric wave disturbances of the vortex and result indeed in a strong polar vortex resembling the dynamic conditions, but not the radiative properties, as were forced by Scaife et al. (2005). The corresponding tropospheric anomaly patterns are different from those found for similar stratospheric conditions without volcanic impact. The most important difference is that the strong warming over Siberia in volcanic winters is missing during strong polar vortex in volcanically-undisturbed winters. If all winters are included in a linear regression analysis, the volcano winters strongly contribute to the result by increasing the statistical significance of anomalies and by partly reversing the anomaly sign over Eurasia (compare panels c and e in Figure 2). We suggest that the position of the strong polar vortex (polar symmetric in the volcanic winters, but displaced to the western NH otherwise) is an important cause of the

600 differences. Strong zonal winds at the edge of the polar vortex in the high latitude upper
601 troposphere over Siberia help maintain and grow baroclinic eddies that transport warm air
602 to Siberia.

603 From our analysis excluding volcanically-disturbed winters we propose a set of hypotheses to
604 explain observed variability on the seasonal time scale considering just a limited number of
605 different mechanisms previously proposed in the scientific literature. We suggest that four
606 processes that are active at the seasonal scale (Figure 11) originating in different NH
607 latitudinal belts and their interaction are sufficient to explain the complexity emerging from
608 the observed climate anomalies:

609 • **Polar latitudes:** Barotropic effects lead to tropospheric pressure anomalies over the
610 Arctic that are similar in sign as in the stratosphere (e.g., Ambaum and Hoskins,
611 2002; Castanheira et al., 2009).

612 • **Mid-latitudes:** Zonal-mean zonal wind anomalies (coming from the stratosphere and
613 penetrating into the troposphere at the edge of the polar vortex) and their
614 interaction with topography lead to wave anomalies projecting on the NAO pattern
615 (e.g., Castanheira et al., 2009). The changed shear of upper tropospheric winds will
616 affect the growth rate of baroclinic eddies and thus feed back to the anomalies of
617 planetary wave's phase and amplitude in the storm track regions (Walter and Graf,
618 2005; Scaife et al., 2012). The latitudinal position of the jet affects the strength of the
619 tropospheric response to the stratospheric polar vortex by determining the strength
620 of the tropospheric eddy feedback (Garfinkel et al., 2013).

621 • **Subtropics:** The subtropical jet can act as active wave guide linking the Pacific with
622 the Atlantic and Europe (e.g., Ambrizzi and Hoskins, 1996; Branstator, 2002). Mainly
623 shorter waves (zonal wave numbers 4 and above) can be trapped by the subtropical
624 jet, while longer waves still can propagate poleward (Jin and Hoskins, 1995). The
625 subtropical jet is enhanced under Central Pacific warming (Kodera, 2010; Graf and
626 Zanchettin, 2012).

627 • **Tropics:** SSTAs in the equatorial Pacific lead to anomalies of precipitation and
628 associated latent heat release affecting the generation and subsequent poleward
629 propagation of Rossby waves (PNA-like response, Jin and Hoskins, 1995). If the

630 subtropical jet wave guide is active during Central Pacific warming, strong
631 teleconnection to the Atlantic and Europe is observed (Graf and Zanchettin, 2012).

632 In polar latitudes we find quite symmetric (with respect to polar vortex strength) anomaly
633 patterns in the troposphere pressure anomalies for strong polar vortex versus weak polar
634 vortex. There are tropospheric negative (positive) pressure anomalies below the strong
635 (weak) polar vortex concentrating over the Canadian Arctic and Greenland (compare Figures
636 3b, 4b, and 5b). A linear framework captures this essential feature (Figure 2f), though it
637 misleadingly highlights a linear signature in the Russian Arctic, which in fact stems from
638 anomalies generated under weak polar vortex and warm ENSO conditions (Figure 5b). This
639 polar latitude link between stratosphere and troposphere can be interpreted as the effect of
640 the stratosphere on tropopause height (Ambaum and Hoskins, 2002) or barotropic
641 adjustment (Castanheira et al., 2009) in polar latitudes. Interaction of the downward
642 penetrating westerly wind anomalies at the edge of the polar vortex with topography
643 (Castanheira et al., 2009) leads to changes in phase and amplitude of high mid-latitude
644 tropospheric planetary waves, supported and extended in time by baroclinic eddy growth
645 rates in the storm track regions of the North Atlantic (Walter and Graf, 2005, 2006;
646 Wittmann et al. 2007; Scaife et al., 2012) projecting preferentially on the NAO pattern. The
647 explanation of the obvious variability may require additional mechanisms. The ENSO-related
648 phase of PNA is a good candidate here as it affects the wind field and, hence, the growth
649 rate of baroclinic eddies over the western part of the North Atlantic. This is a possible
650 explanation why the Aleutian Low and the Icelandic Low are positively correlated during
651 strong polar vortex (Quadrelli and Wallace, 2002, looking only at surface pressure-based
652 Northern Annular Mode; Castanheira and Graf, 2003, looking at the coupled stratosphere-
653 troposphere system), but not during weak polar vortex. Ineson and Scaife (2009) and
654 Toniazzo and Scaife (2006) concluded that only moderate El Niños lead to negative NAO,
655 while strong El Niños produce similar sea-level pressure anomalies as they are observed in
656 winters without strong stratospheric warming events. Their results, however, are strongly
657 related to their choice of the Niño3 index, which gives warming in the East Pacific higher
658 weight than to SSTAs in the Central Pacific. Their “moderate” El Niños are therefore more
659 biased towards warming in the Central Pacific, where already small SSTAs result in strong

660 increase of precipitation and atmospheric heating (see Figure 2b of Toniazzo and Scaife
661 (2006)), hence a stronger Aleutian Low as discussed in Graf and Zanchettin (2012).

662 It is also necessary to find an explanation for the concentration of the observed pressure
663 anomalies on the Western Hemisphere. Kodera (2010, his Figure 3) showed regression
664 patterns of surface pressure with the Niño3.4 index that match the PNA pattern with high
665 pressure at the Aleutian Low and low pressure over the Canadian Arctic during cold ENSO
666 events, and vice versa for warm ENSO. Hence, we observe a mix of tropospheric and
667 stratospheric impacts on the polar and sub-polar latitude NH pressure field. Under weak
668 polar vortex and cold ENSO conditions, positive tropospheric pressure anomalies develop
669 less strongly over the pole and the Canadian Arctic. The significant Arctic positive pressure
670 anomaly is clearly located to the east of Greenland, but still in latitudes covered by the weak
671 stratospheric polar vortex. Possibly, this is due to the superposing effects of the tropospheric
672 PNA, which is impacted by the state of ENSO, and the anomalous stratospheric circulation.
673 When a weak polar vortex coincides with cold ENSO, the negative pressure anomaly over the
674 Canadian Arctic (negative PNA) in part cancels the positive pressure anomaly induced by the
675 stratosphere leading to destructive superposition. Conversely, since (nearly) all very strong
676 polar vortex winters occurred during cold ENSO, the strong negative pressure anomalies over
677 the Canadian Arctic can be interpreted as a constructive superposition of the ENSO-related
678 negative PNA with the stratosphere-related low pressure in Arctic latitudes. A similar
679 interaction, but with opposite sign, sets in during weak polar vortex and warm ENSO
680 conditions. Then we have a constructive superposition of a positive phase of the PNA and
681 stratosphere-related high Arctic pressure, resulting in very high pressure over the Canadian
682 Arctic.

683 The mid-latitude tropospheric pressure anomalies and the related temperature anomalies
684 are relatively weak in non-volcanic winters under cold ENSO conditions (Figures 3b and 4b),
685 but are very strong and extensive under weak polar vortex and warm ENSO conditions
686 (Figure 5b). The respective years are all Central Pacific or hybrid El Niño years (compare
687 Johnson, 2013) with enhanced tropical precipitation at and to the west of the dateline. The
688 interpretation of the anomaly patterns can therefore closely follow the argumentation of
689 Graf and Zanchettin (2012): Central Pacific warming leads to stronger convective
690 precipitation and latent heat release over a wide longitudinal range, resulting in a positive

691 phase of the PNA with enhanced westerlies at the southern flank of the stronger-than-
692 normal Aleutian Low. The enhanced westerlies merge with and extend the East Asian
693 subtropical jet that evolves in December. This acts as an active upper tropospheric
694 subtropical wave guide for shorter wave disturbances originating from the tropics (the
695 "subtropical bridge") and a weaker than normal Azores High. Simultaneously, reduced zonal
696 winds penetrating from the stratosphere to the troposphere at the edge of the polar vortex
697 lead to weaker interaction of the zonal-mean flow with topography in high mid-latitudes and
698 to less growth of baroclinic eddies resulting in a weaker-than-normal Icelandic Low and
699 North Atlantic storm track (Walter and Graf, 2005, 2006; Scaife et al., 2012, sea also the
700 discussion in Gerber et al. 2012). Both mechanisms together promote a negative phase of
701 the NAO. The related tropospheric anomalies are more extensive and of larger scale. They
702 provide much clearer patterns than during winters with weak polar vortex and cold ENSO
703 conditions or during strong polar vortex, also under cold ENSO conditions, when the
704 subtropical bridge is not activated.

705

706 **5. Conclusions**

707 The tropospheric mid-winter signature of the Northern Hemisphere's stratospheric polar
708 vortex in NCEP/NCAR reanalysis data for the last 65 years exhibits elements of linearity only
709 over the Arctic due to barotropic adjustment. In subpolar and lower latitudes linearity is
710 disturbed by tropospheric anomalies related especially to the ENSO state. Furthermore,
711 anomalous patterns reveal fundamental differences in the observed tropospheric and near-
712 surface signature of a strong polar vortex under volcanically-disturbed and volcanically-
713 undisturbed conditions, especially concerning the warming pattern over the Eurasian
714 continent. It is, therefore, not recommended to include volcanically-disturbed winters in an
715 observation-based analysis dedicated to investigate the effect of polar vortex strength on
716 tropospheric climate. In the absence of additional tropospheric forcings, volcanically
717 disturbed winters might allow to study the pure effects of enhanced stratospheric polar
718 vortex on tropospheric variability. However, in these cases the caveat of concurrently having
719 radiative forcing from the volcanic aerosols in the stratosphere and in the troposphere still
720 exists and needs to be considered.

The sampling of winters with strong polar vortex is clearly dominated by cold ENSO and, to a lesser extent, westerly QBO. The strongest climate anomalies during Northern Hemisphere winters occur when a weak polar vortex coincides with warm Central Pacific ENSO conditions. This is interpreted such that these coincident states of warm ENSO and of weak polar vortex induce constructively-superposing anomalous tropospheric patterns that result in a strong negative phase of the NAO, and associated cooling over Eurasia. In contrast, climate anomalies are the weakest during Northern Hemisphere winters with weak polar vortex and cold ENSO, due to destructive superposition of associated tropospheric anomalies.

Although our statistical analysis of reanalyzed atmospheric data shows statistically significant differences in boreal mid-winter climate between groups of strong and weak polar vortex at cold ENSO, warm and cold ENSO at weak polar vortex as well as between volcanic and non-volcanic winters at strong polar vortex, we must be very cautious with drawing conclusions about underlying mechanisms. The lengths of observational/reanalysis data series still are too short to allow for conclusive statements about the dominant source of winter regional climate variability in the Northern Hemispheres. The number of processes involved in the stratosphere, the troposphere and the coupled ocean-atmosphere system, and the complexity of their interactions lead, at best, to small samples if one tries to disentangle the individual contributions through composite analysis. So, on the one hand, this renders inferences about dynamics based on derived anomalous patterns strongly subject to sampling biases. On the other hand, this study reveals that such a separation is physically justified, and hence necessary. Full observational-period statistics would misleadingly smear out dynamically different tropospheric process signatures, rather than highlighting one single imprint from a noisy signal. Comparative analysis of numerical model results with observation/reanalysis must therefore account for biases in the latter, i.e., account for the empirical sampling distribution of (at least) polar vortex strength, ENSO state and QBO phase derived from observations. Only in a second step, dedicated numerical experiments with well tested models could then provide reliable information about stratosphere-troposphere coupling processes and about the tropospheric and near-surface winter signature of the Northern Hemisphere stratospheric polar vortex.

Acknowledgements: This work benefits from stimulating visits that Hans-F Graf spent at the Max Planck Institute for Meteorology. The authors would like to thank Elisa Manzini and two anonymous reviewers for helpful comments on an earlier version of this paper. This work was supported by the Federal Ministry for Education and Research in Germany (BMBF) through the research program “MiKlip” (FKZ:01LP1158A(DZ):/01LP1130A(CT,MB)).

References

Ambaum, M. H. P. and Hoskins, B. J., 2002: The NAO troposphere stratosphere connection, J. Climate, 15, 1969–1978

Ambrizzi, T., and B. J. Hoskins, 1997: Stationary Rossby-wave propagation in a baroclinic atmosphere, Q. J. R. Meteorol. Soc., 123(540), 919–928, doi:10.1002/qj.49712354007

Baldwin, M. P., Cheng, X. H., and Dunkerton, T. J., 1994: Observed relations between winter-mean tropospheric and stratospheric circulation anomalies, Geophys. Res. Lett., 21, 1141–1144

Baldwin, M. P., and T. J. Dunkerton, 2001: Stratospheric harbingers of anomalous weather regimes. Science, 294, 581–584

Branstator, G., 2002: Circumglobal teleconnections, the jet stream waveguide, and the North Atlantic oscillation. J. Clim., 15, 1893–1910, doi:10.1175/1520 0442(2002)015<1893:CTTJSW>2.0.CO;2.

Brönnimann, S., 2007: Impact of El Niño-Southern Oscillation on European climate. Reviews of Geophysics, 45 RG3003, doi:10.1029/2006RG000199.

Butler, A. H., and L. M. Polvani, 2011: El Niño, La Niña, and stratospheric sudden warmings: A reevaluation in light of the observational record, Geophys. Res. Lett., 38, L13807, doi:10.1029/2011GL048084.

784 Cagnazzo, C., and E. Manzini, 2009: Impact of the stratosphere on the winter tropospheric
785 teleconnectionsbetween ENSO and the North Atlantic and European region. J. Climate, 22,
786 1223–1238
787
788 Camp, C. D., and K.-K. Tung, 2007: Stratospheric polar warming by ENSO in winter: A
789 statistical study, Geophys. Res. Lett., 34, L04809, doi:10.1029/2006GL028521
790 Castanheira, J.M. and H.-F. Graf, 2003: North Pacific - North Atlantic relationships under
791 stratospheric control? J. Geophys. Res., Vol.108, D1, 4036, doi :10.1029/2002JD002754, 2003
792 Castanheira, J.M., Liberato, M.L.R., de la Torre, L., and H.-F. Graf, 2009: Baroclinic Rossby
793 Wave Forcing and Barotropic Rossby Wave Response to Stratospheric Vortex Variability, J.
794 Atmos. Sci., 66, 4 , 902-914
795 Charlton-Perez, A. J., et al., 2013: On the lack of stratospheric dynamical variability in low-
796 top versions of the. CMIP5 models, J. Geophys. Res. Atmos. Volume 118, 6, 2494–2505
797
798 Cohen, J., M. Barlow, P. J. Kushner, and K. Saito, 2007: Stratosphere– troposphere coupling
799 and links with Eurasian land surface variability. J. Climate, 20, 5335–5343.
800
801 Driscoll, S., A. Bozzo, L. J. Gray, A. Robock, and G. Stenchikov, 2012: Coupled Model
802 Intercomparison Project 5 (CMIP5) Simulations of Climate Following Volcanic Eruptions, J.
803 Geophys. Res., 117, D17105, doi:10.1029/2012JD017607.
804
805 Fletcher, C. G., and P. J. Kushner, 2011: The role of linear interference in the Annular Mode
806 response to tropical SST forcing, J. Climate, 24(3), 778-794
807
808 Garfinkel, C.I., and D.L. Hartmann, 2007: Effects of the El-Nino Southern Oscillation and the
809 Quasi-Biennial Oscillation on polar temperatures in the stratosphere, J. Geophys. Res.
810 Atmos., 112, D19112, doi:10.1029/2007JD008481.
811
812 Garfinkel, C.I., Hartmann, D.L., 2008: Different ENSO teleconnections and their effects on the
813 stratospheric polar vortex. J Geophys Res Atmos 113. doi:10.1029/2008JD009920

814 Garfinkel, C.I., and Hartmann, D.L., 2010: Influence of the quasi-biennial oscillation on the
815 North Pacific and El-Niño teleconnections. J Geophys Res 115:D20116.
816 doi:10.1029/2010JD014181
817
818 Garfinkel, C. I., M. M. Hurwitz, D. W. Waugh, A.H. Butler (2012), Are the Teleconnections of
819 Central Pacific and Eastern Pacific El Nino Distinct in Boreal Wintertime?, Clim. Dynam.,
820 doi:10.1007/s00382-012-1570-2.
821
822 Garfinkel, C.I., D. W. Waugh, E. P. Gerber, 2013: The Effect of Tropospheric Jet Latitude on
823 Coupling between the Stratospheric Polar Vortex and the Troposphere . J. Clim, 26, 2077-
824 2095
825
826 Gerber, E. P., and L. M. Polvani, 2009: Stratosphere–troposphere coupling in a relatively
827 simple AGCM: The importance of stratospheric variability. J. Climate, 22, 1920–1933.
828
829 Gerber, Edwin P., et al., 2012: Assessing and Understanding the Impact of Stratospheric
830 Dynamics and Variability on the Earth System. Bull. Amer. Meteor. Soc., 93, 845–859. doi:
831 http://dx.doi.org/10.1175/BAMS-D-11-00145.1

832 Graf, H.-F.; I. Kirchner; A. Robock and I. Schult, 1993: Pinatubo eruption winter climate
833 effects: Model versus observation. Clim. Dynam., 9, 81-93

834 Graf, H.-F., Perlwitz, J., and Kirchner, I., 1994: Northern Hemisphere tropospheric mid-
835 latitude circulation after violent volcanic eruptions, Contributions to Atmospheric Physics,
836 67, 3–13
837
838 Graf, H.-F., Q. Li, and M.A. Giorgetta, 2007: Volcanic effects on climate: Revisiting the
839 mechanisms. Atmos. Chem. Phys., 7, 4503-4511

840 Graf, H.-F., and D. Zanchettin, 2012: Central Pacific El Nino, the subtropical bridge, and
841 Eurasian climate. J Geophys Res 117. doi:10.1029/2011JD016493
842

843 Hegyi, B. M., and Y. Deng, 2011: A dynamical fingerprint of tropical Pacific sea surface
844 temperatures on the decadal-scale variability of cool-season Arctic precipitation. Journal of
845 Geophysical Research, 116(D20), D20121.
846
847 Hurwitz, M.M., P.A. Newman, and C.I. Garfinkel, 2012: On the Influence of North Pacific Sea
848 Surface Temperatures on the Arctic Winter Climate, J. Geophys. Res. Atmos., 117, D19110,
849 doi:10.1029/2012JD017819.
850
851 Ineson, S., and A. A. Scaife, 2009: The role of the stratosphere in the European climate
852 response to El Niño. Nat. Geosci., 2, 32–36.
853
854 Jin, F.F., and B.J. Hoskins, 1995: The direct response to tropical heating in a baroclinic
855 atmosphere, J. Atmos. Sci., 52, 307-319
856
857 Johnson, N., 2013: How many ENSO flavors can we distinguish? J. Climate, 26, 4816–4827,
858 doi:10.1175/JCLI-D-12-00649.1
859
860 Kalnay, E., and Coauthors, 1996: The NCEP/NCAR 40-Year Reanalysis Project. Bull. Amer.
861 Meteor. Soc., 77, 437–471
862
863 Kodera, K., M. Chiba, H. Koide, A. Kitoh, and Y. Nikaidou, 1996: Interannual variability of the
864 winter stratosphere and troposphere, J. Meteor. Soc. Japan, 74, 365-382
865
866 Kodera, K., 2010: Change in the ENSO Teleconnection Characteristics in the Boreal Winter,
867 SOLA, Vol. 6A, 021−024, doi:10.2151/sola.6A-006

868 Li, J.,S.-P. Xie, E. R. Cook, M. S. Morales, D. A. Christie, N. C. Johnson, F. Chen, R. D'Arrigo, A.
869 M. Fowler, X. Gou, and K. Fang, 2013: El Niño modulations over the past seven centuries.
870 Nature Cl. Ch., 3:9, 822-826, doi:10.1038/NCLIMATE1936

871 van Loon, H., and K. Labitzke, 1987: The Southern Oscillation. Part V: The Anomalies in the
872 Lower Stratosphere of the Northern Hemisphere in Winter and a Comparison with the

873 Quasi-Biennial Oscillation. *Mon. Wea. Rev.*, **115**, 357–369. doi: http://dx.doi.org/10.1175/1520-
874 0493(1987)115<0357:TSOPVT>2.0.CO;2

875

876 Manzini, E., M. A. Giorgetta, M. Esch, L. Kornblueh, E. Roeckner, 2006: The Influence of Sea
877 Surface Temperatures on the Northern Winter Stratosphere: Ensemble Simulations with the
878 MAECHAM5 Model. J. Climate, **19**, 3863–3881. doi: http://dx.doi.org/10.1175/JCLI3826.1

879 Morgenstern, O., et al. (2010), Anthropogenic forcing of the Northern Annular Mode in
880 CCMVal-2 models, J. Geophys. Res., 115, *D00M03,* doi:10.1029/2009JD013347.
881
882 Perlwitz, J., and H.-F. Graf, 1995: The statistical connection between tropospheric and
883 stratospheric circulation of the Northern Hemisphere in winter, J. Climate, 8, 2281–2295
884
885 Perlwitz, J., and N. Harnik, 2004: Downward coupling between the stratosphere and
886 troposphere: The relative roles of wave and zonal mean processes. J. Climate, 17, 4902–
887 4909.
888
889 Polvani, L.M., and D.W. Waugh, 2004: Upward wave activity flux as a precursor to extreme
890 stratospheric events and subsequent anomalous surface weather regimes. J Clim 17:3548–
891 3554
892
893 Quadrelli, R., and J. M. Wallace, 2002: Dependence of the structure of the Northern
894 Hemisphere annular mode on the polarity of ENSO. Geophysical Research Letters, 29(23),
895 47-1.
896
897 Robock, A., 2000: Volcanic eruptions and climate, REVIEWS OF GEOPHYSICS, Volume: 38, 2,
898 191-219 DOI: 10.1029/1998RG000054

899 Scaife, A. A., J. R. Knight, G. K. Vallis, and C. K. Folland, 2005: A stratospheric influence on the
900 winter NAO and North Atlantic surface climate. Geophys. Res. Lett., 32, L18715, doi:10.1029/
901 2005GL023226
902

903 Scaife, A. A ., et al., 2012: Climate change projections and stratosphere–troposphere
904 Interaction. Clim. Dynam. , 38:2089–2097, DOI 10.1007/s00382-011-1080-7
905
906 Schimanke, S., Körper, J., Spangehl, T., Cubasch, U., 2011: Multi-decadal variability of sudden
907 stratospheric warmings in an AOGCM, Geophys. Res. Lett., 38, 1, 1944-8007,
908 doi.org/10.1029/2010GL045756
909
910 Stenchikov, G., K. Hamilton, R. J. Stouffer, A. Robock, V. Ramaswamy, B. Santer, and H.-F. Graf, 2006:
911 Arctic Oscillation response to Volcanic Eruptions in the IPCC AR4 Climate Models, J. Geophys. Res.,
912 111, D07107, doi:10.1029/2005JD006286
913
914 Taguchi, M., and D. L. Hartmann, 2005: Interference of extratropical surface climate
915 anomalies induced by El Nino and stratospheric sudden warmings. Geophysical Res. Lett., 32,
916 L04709, doi:10.1029/2004GL022004.
917
918 Toniazzo, T., and A. A. Scaife, 2006: The influence of ENSO on winter North Atlantic climate,
919 Geophys. Res. Lett., 33, *L24704,* doi:10.1029/2006GL027881.
920
921 Walter, K., and H.-F. Graf, 2002: On the changing nature of the regional connection between
922 the North Atlantic Oscillation and sea surface temperature, J. Geophys. Res., 107 (D17),
923 4338, doi: 10.1029/2001JD000850
924 Walter, K., and H.-F. Graf, 2005: The North Atlantic variability structure, storm tracks, and
925 precipitation depending on the polar vortex strength. *Atmos. Chem. Phys.*, **5,** 239–248. SRef-
926 ID: 1680-7324/acp/2005-5-239
927
928 Walter, K., and H.-F. Graf, 2006: Life cycles of North Atlantic teleconnections under strong
929 and weak polar vortex conditions, *Q. J. R. Meteorol. Soc.* (2006), **132**, pp. 467–483 doi:
930 10.1256/qj.05.25
931
932 Wei, K., W. Chen, and R. Huang (2007), Association of tropical Pacific sea surface
933 temperatures with the stratospheric Holton-Tan Oscillation in the Northern Hemisphere
934 winter, Geophys. Res. Lett., 34, L16814, doi:10.1029/2007GL030478

935

936 Wittman, M. A. H., L. M. Polvani, R. K. Scott, and A. J. Charlton, 2004: Stratospheric influence
937 on baroclinic lifecycles and its connection to the Arctic Oscillation. Geophys. Res. Lett., 31,
938 L16113, doi:10.1029/2004GL020503.

939

940 Wittman, M. A. H., A. J. Charlton, and L. M. Polvani, 2007: The Effect of Lower Stratospheric
941 Shear on Baroclinic Instability. *J. Atmos. Sci.*, **64**, 479–496. doi:
942 http://dx.doi.org/10.1175/JAS3828.1

943

944 Zanchettin, D., C. Timmreck, H.-F. Graf, A. Rubino, S. Lorenz, K. Lohmann, K. Krueger, and J. H.
945 Jungclaus, 2012: Bi-decadal variability excited in the coupled ocean–atmosphere system by
946 strong tropical volcanic eruptions. Clim. Dyn., 39:1-2, 419-444, DOI:10.1007/s00382-011-
947 1167-1

Tables

		ENSO	
		WARM	COLD/NEUTRAL
Polar Vortex	STRONG	**-05**	+67, **-72**, **-74**, **-76**, **+89**, +90, **-96**, -97, **+00**
	WEAK	**+58**, **+70**, **-77**, **-87**, **-10**	+60, **-85**, +04, -06, -09, -13

Table 1 - Distribution of strong and weak polar vortex winters (JF) versus state of ENSO (Oceanic Niño Index) in DJ, phase of November QBO, and 10.7 cm solar activity index. Numbers indicate the last two digits of the year. High (low) solar activity indicated by +(-). Small numbers mean that ENSO index is only weakly positive or negative, bold numbers indicate ENSO warm or cold phase. QBO phase in November before: west in red, east in black and neutral in green.

Figure captions

Figure 1 – Top: time series of Polar Vortex Index (PVI) for the Northern Hemisphere. Bottom: time series of the ENSO index (see methods for details). The horizontal red dashed lines indicate the thresholds used to identify strong and weak PVI states, and cold and warm ENSO states. Blue circles indicate volcanically-disturbed winters characterized by a strong polar vortex.

Figure 2 - Linear regression coefficients of mid-winter (JF) 50-hPa (panels a,e) and 500 hPa (b,f) geopotential heights, 1000 hPa air temperature (c,g) and Pacific sea-surface temperatures (d,h) on the PVI index (see methods) for the full period (a-d) and excluding volcanically-affected winters (e-h). Data are NCAR/NCEP reanalyses covering the period 1948-2013. Statistically non-significant statistics are stippled (see methods). Data are linearly detrended prior to regression analysis.

Figure 3 - Anomaly patterns of mid-winter (JF) 50-hPa (panel a) and 500 hPa (b) geopotential heights, 1000 hPa air temperature (c) and Pacific sea-surface temperatures (d) under strong polar vortex and cold ENSO conditions (years: 1972 1974 1976 1989 1996 1997 2000). Statistically non-significant anomalies are stippled.

Figure 4 - Anomaly patterns of mid-winter (JF) 50-hPa (panel a) and 500 hPa (b) geopotential heights, 1000 hPa air temperature (c) and Pacific sea-surface temperatures (d) under weak polar vortex and cold ENSO conditions (years: 1985 2006 2009 2013). Statistically non-significant anomalies are stippled.

Figure 5 – Differences between average patterns of mid-winter (JF) 50-hPa (panel a) and 500 hPa (b) geopotential heights, 1000 hPa air temperature (c) and Pacific sea-surface temperatures (d) under strong and weak polar vortex conditions, both concomitant with cold ENSO (i.e., difference between patterns in Figures 3 and 4). Statistically non-significant anomalies are stippled.

1003

1004 Figure 6 - Anomaly patterns of mid-winter (JF) 50-hPa (panel a) and 500 hPa (b) geopotential
1005 heights, 1000 hPa air temperature (c) and Pacific sea-surface temperatures (d) under weak
1006 polar vortex and warm ENSO conditions (years: 1958 1970 1977 1987 2010). Statistically
1007 non-significant anomalies are stippled.

1008

1009 Figure 7 – Differences between average patterns of mid-winter (JF) 50-hPa (panel a) and 500
1010 hPa (b) geopotential heights, 1000 hPa air temperature (c) and Pacific sea-surface
1011 temperatures (d) under warm and cold ENSO conditions, both concomitant with a weak
1012 polar vortex (i.e., difference between patterns in Figures 6 and 4). Statistically non-
1013 significant anomalies are stippled.

1014

1015 Figure 8 - Anomaly patterns of mid-winter (JF) 50-hPa (panel a) and 500 hPa (b) geopotential
1016 heights, 1000 hPa air temperature (c) and Pacific sea-surface temperatures (d) under strong
1017 polar vortex conditions affected by volcanic aerosols (years: 1964 1983 1984 1993). All
1018 winters are included. Statistically non-significant anomalies are stippled.

1019

1020 Figure 9 - Differences between average patterns of mid-winter (JF) 50-hPa (panel a) and 500
1021 hPa (b) geopotential heights, 1000 hPa air temperature (c) and Pacific sea-surface
1022 temperatures (d) under strong polar vortex conditions in volcanically-disturbed and
1023 volcanically-undisturbed winters. All winters are included. Statistically non-significant
1024 anomalies are stippled.

1025

1026 Figure 10 - Anomaly patterns of mid-winter (JF) 850-hPa zonal wind under strong polar
1027 vortex conditions in winters not affected (panel a, years: 1972 1974 1976 1989 1996 1997
1028 2000) and winters affected by volcanic aerosols (panel b, years: 1964 1983 1984 1993), and
1029 difference between the two (c). Analysis as for Figures 3 and 8, respectively. Statistically non-
1030 significant anomalies are stippled.

1031

1032 Figure 11 - Cartoon of the proposed mechanisms involved in creating observed climate
1033 anomalies in Northern Hemisphere winters.

1034

Figure

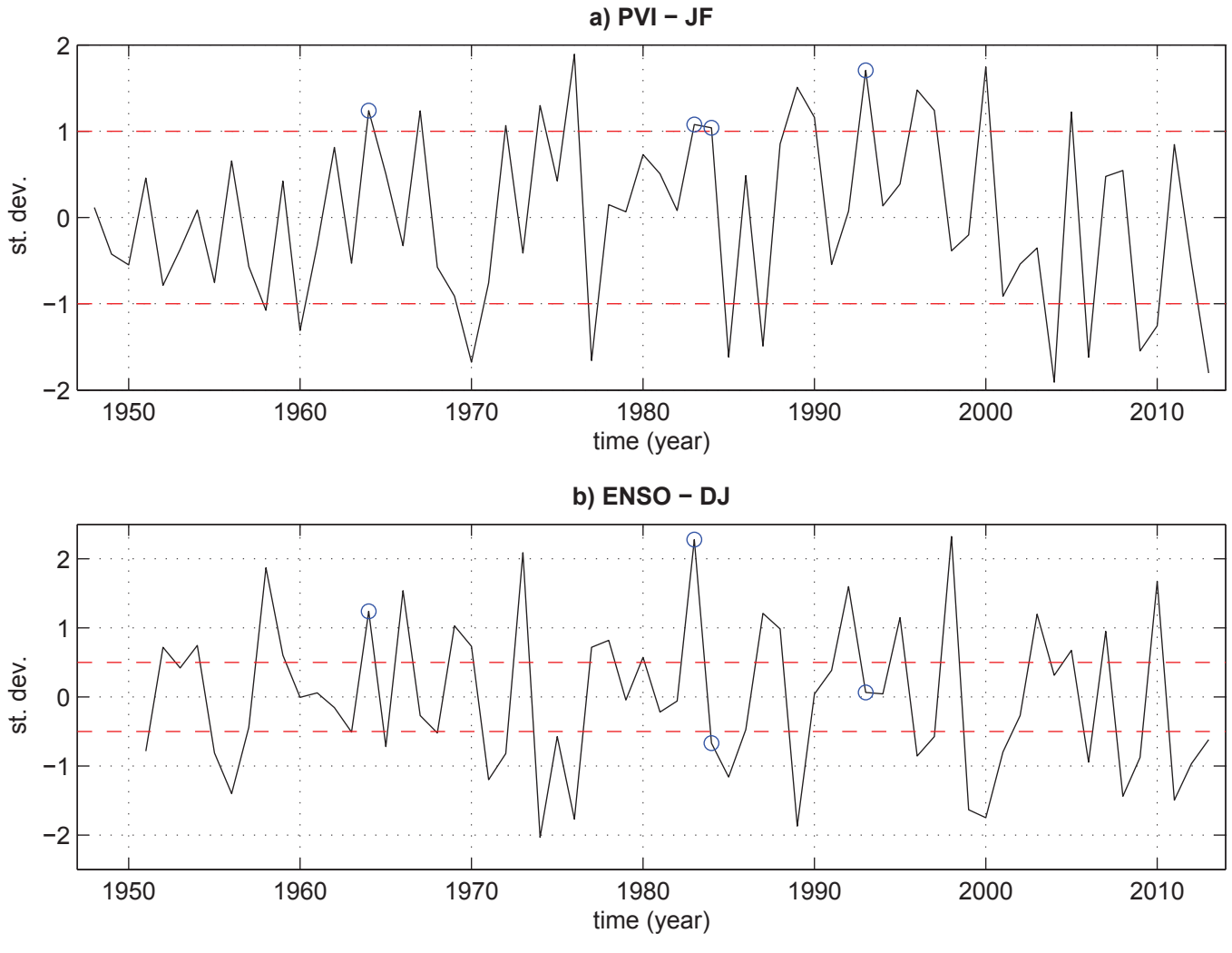
a) PVI − JF
st. dev.
time (year)
b) ENSO − DJ
st. dev.
time (year)
1950
1960
1970
1980
1990
2000
2010

Figure

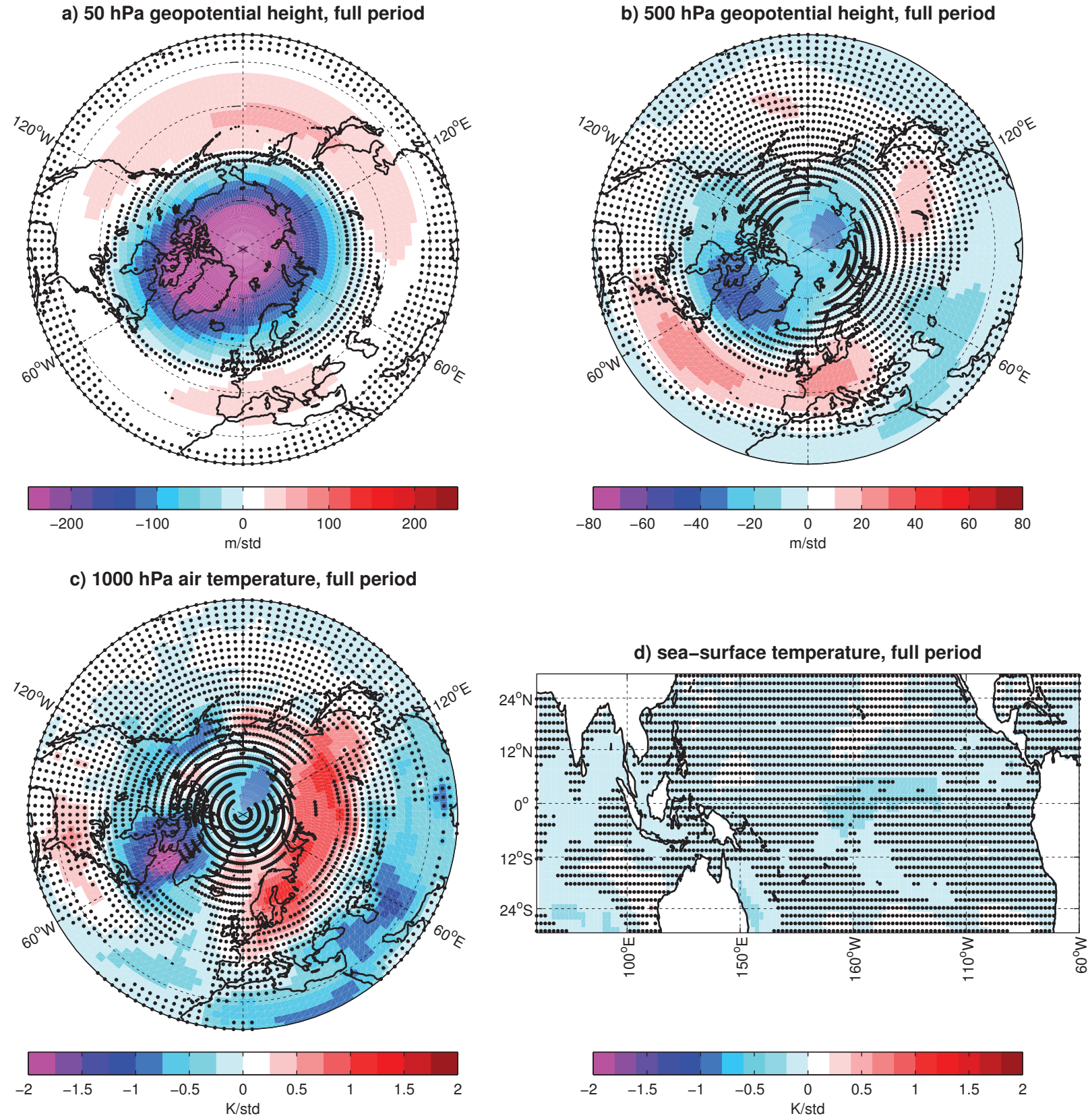
a) 50 hPa geopotential height, full period
120°W
120°E
60°W
60°E
−200
−100
0
100
200
m/std
b) 500 hPa geopotential height, full period
120°W
120°E
60°W
60°E
−80
−60
−40
−20
0
20
40
60
80
m/std
c) 1000 hPa air temperature, full period
120°W
120°E
60°W
60°E
−2
−1.5
−1
−0.5
0
0.5
1
1.5
2
K/std
d) sea−surface temperature, full period
24°N
12°N
0°
12°S
24°S
100°E
150°E
160°W
110°W
60°W
−2
−1.5
−1
−0.5
0
0.5
1
1.5
2
K/std

Figure

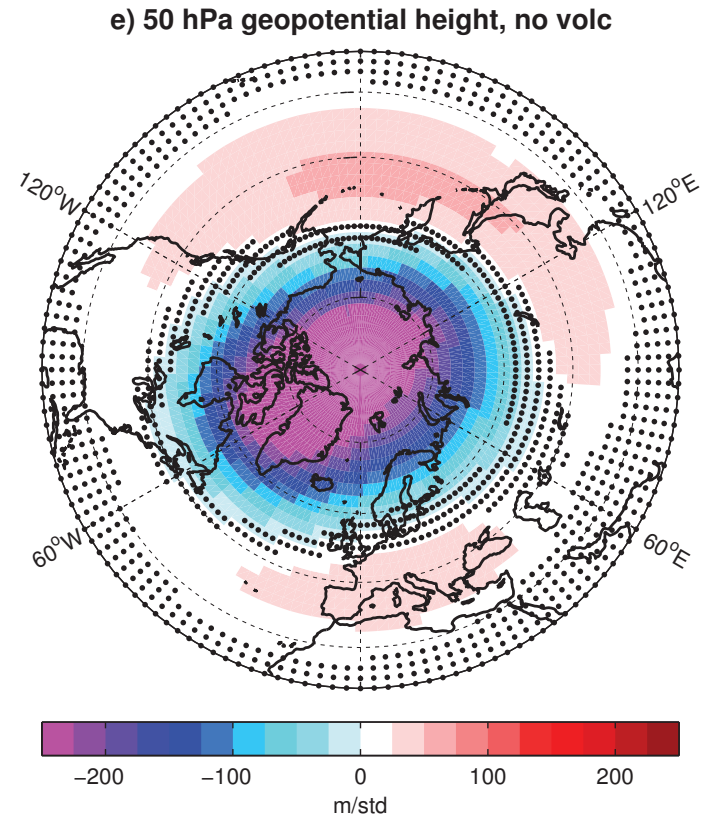
e) 50 hPa geopotential height, no volc
120°W
120°E
60°W
60°E
−200
−100
0
100
200
m/std

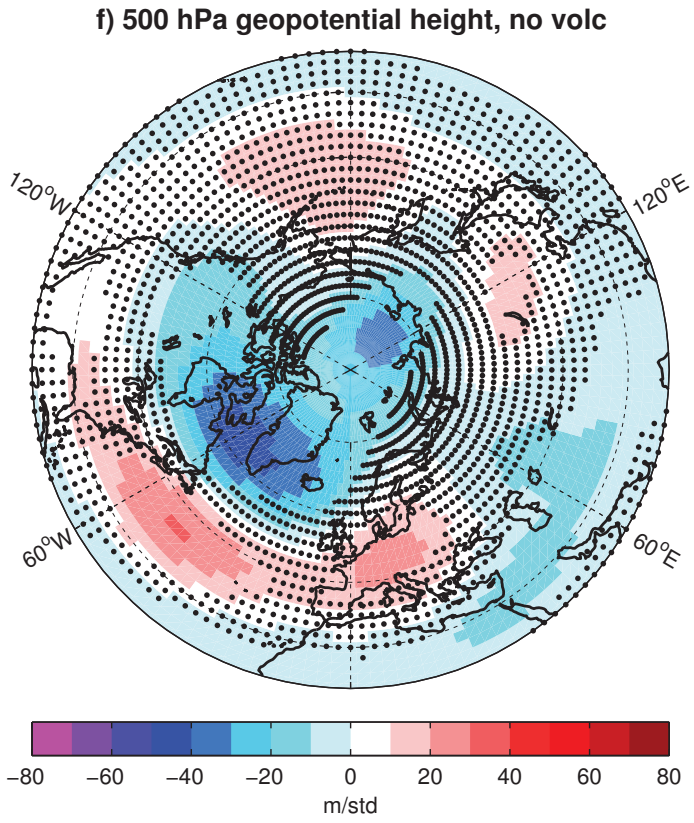
f) 500 hPa geopotential height, no volc
120°W
120°E
60°W
60°E
−80
−60
−40
−20
0
20
40
60
80
m/std

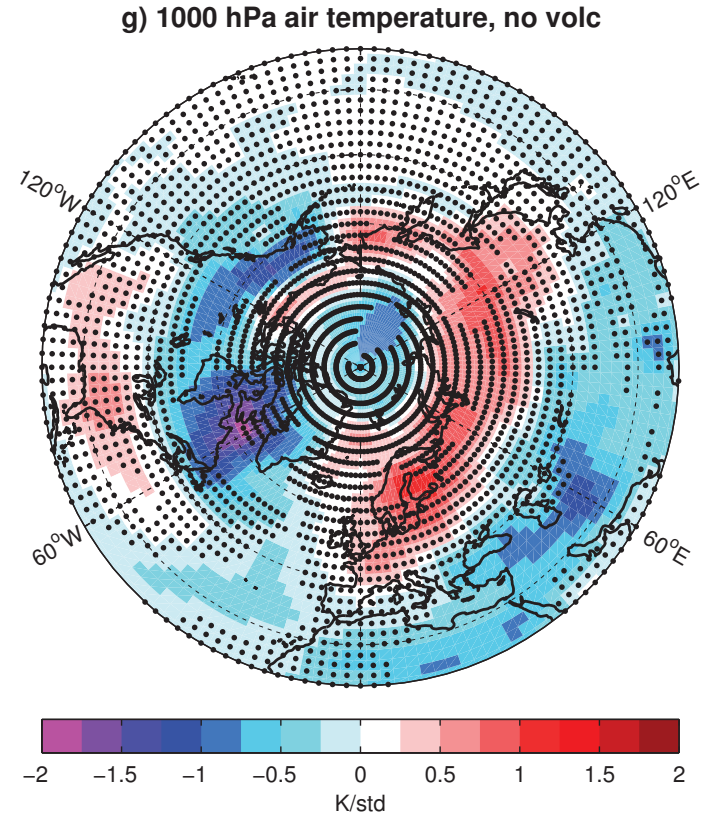
g) 1000 hPa air temperature, no volc
120°W
120°E
60°W
60°E
−2
−1.5
−1
−0.5
0
0.5
1
1.5
2
K/std

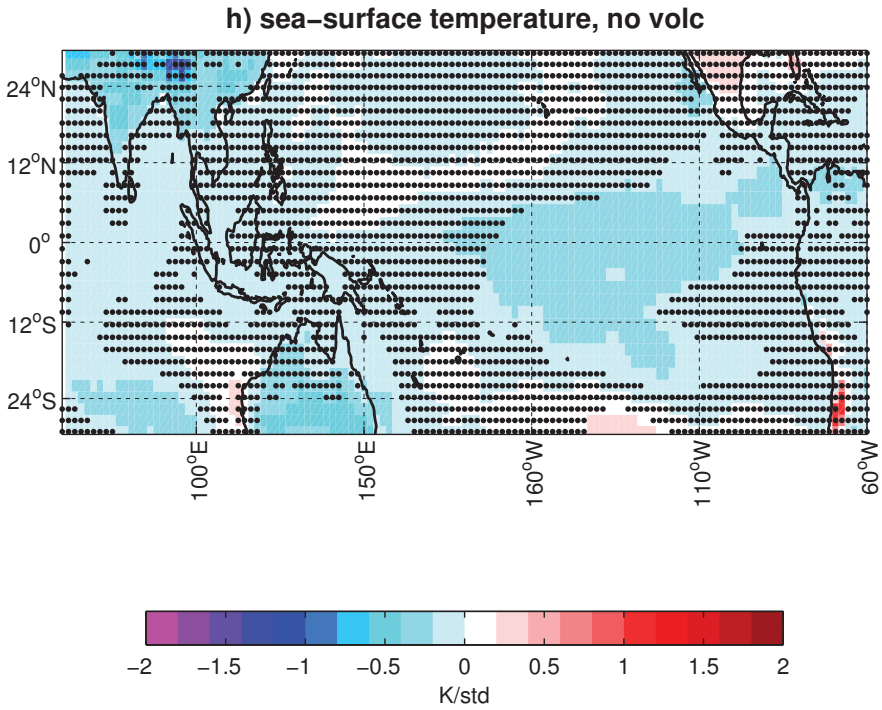
h) sea−surface temperature, no volc
24°N
12°N
0°
12°S
24°S
100°E
150°E
160°W
110°W
60°W
−2
−1.5
−1
−0.5
0
0.5
1
1.5
2
K/std

Figure

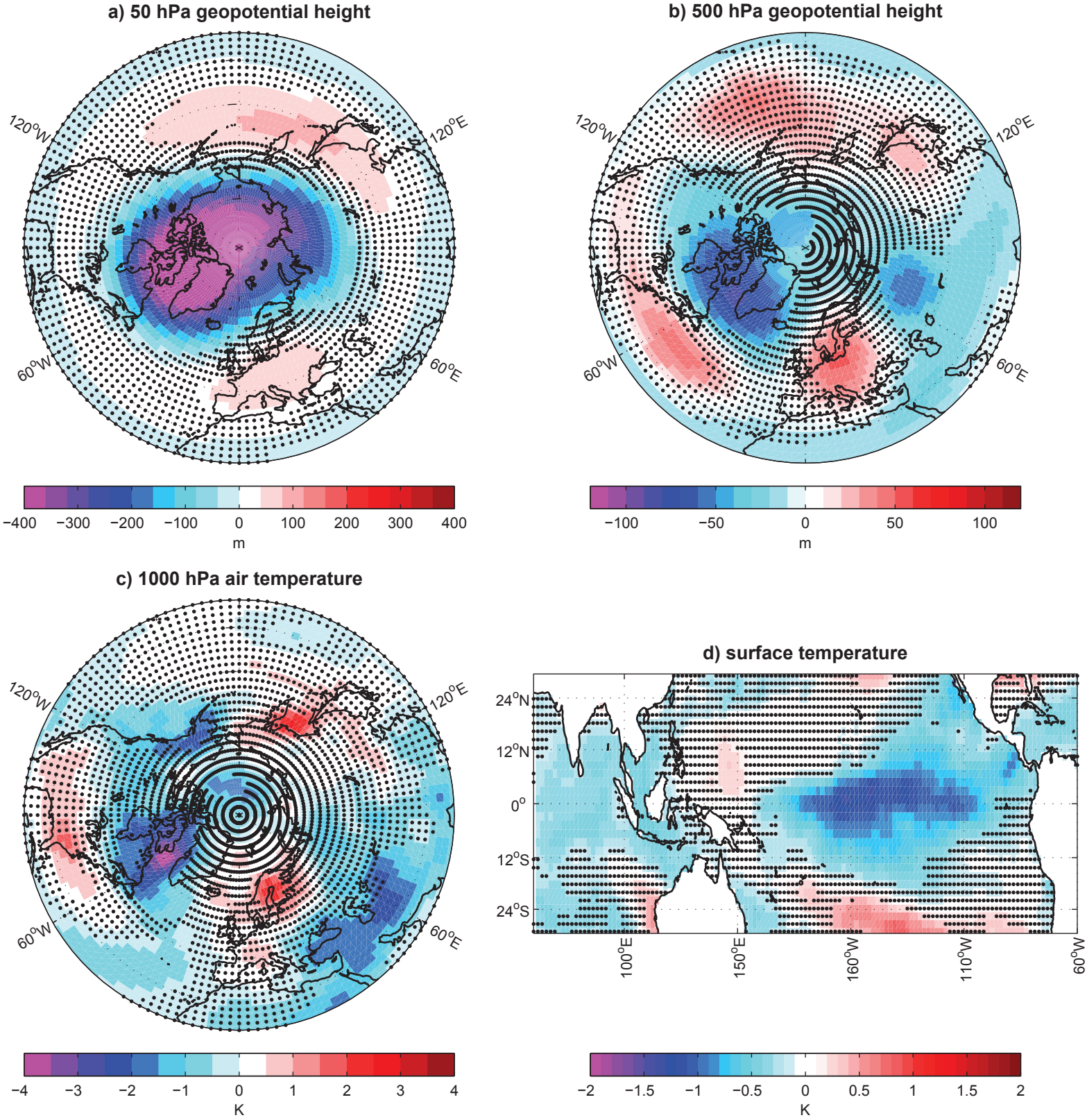
a) 50 hPa geopotential height
120°W
120°E
60°W
60°E
−400 −300 −200 −100 0 100 200 300 400
m
b) 500 hPa geopotential height
120°W
120°E
60°W
60°E
−100 −50 0 50 100
m
c) 1000 hPa air temperature
120°W
120°E
60°W
60°E
−4 −3 −2 −1 0 1 2 3 4
K
d) surface temperature
24°N
12°N
0°
12°S
24°S
100°E
150°E
160°W
110°W
60°W
−2 −1.5 −1 −0.5 0 0.5 1 1.5 2
K

Figure

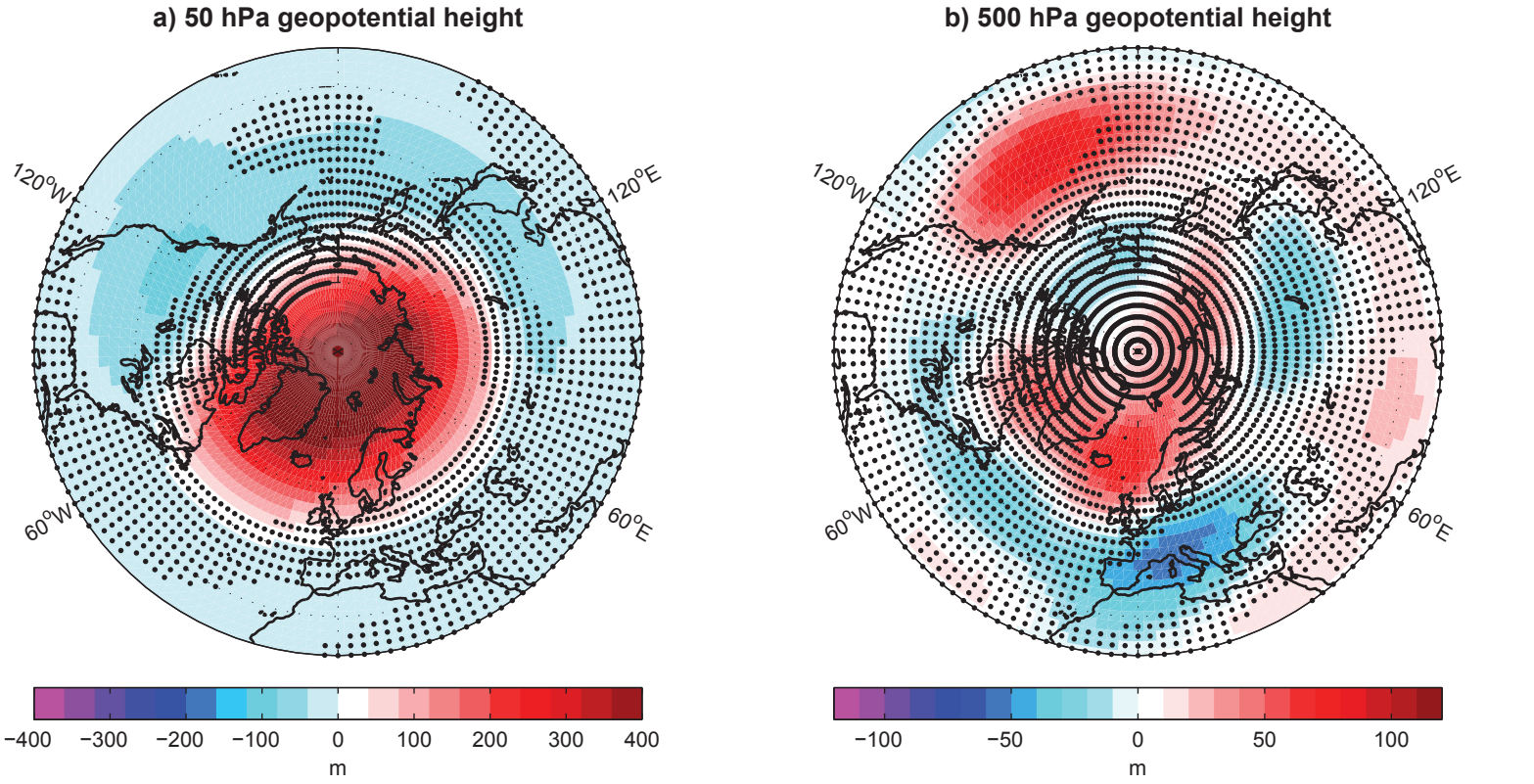
a) 50 hPa geopotential height
120°W
120°E
60°W
60°E
−400 −300 −200 −100 0 100 200 300 400
m
b) 500 hPa geopotential height
120°W
120°E
60°W
60°E
−100 −50 0 50 100
m

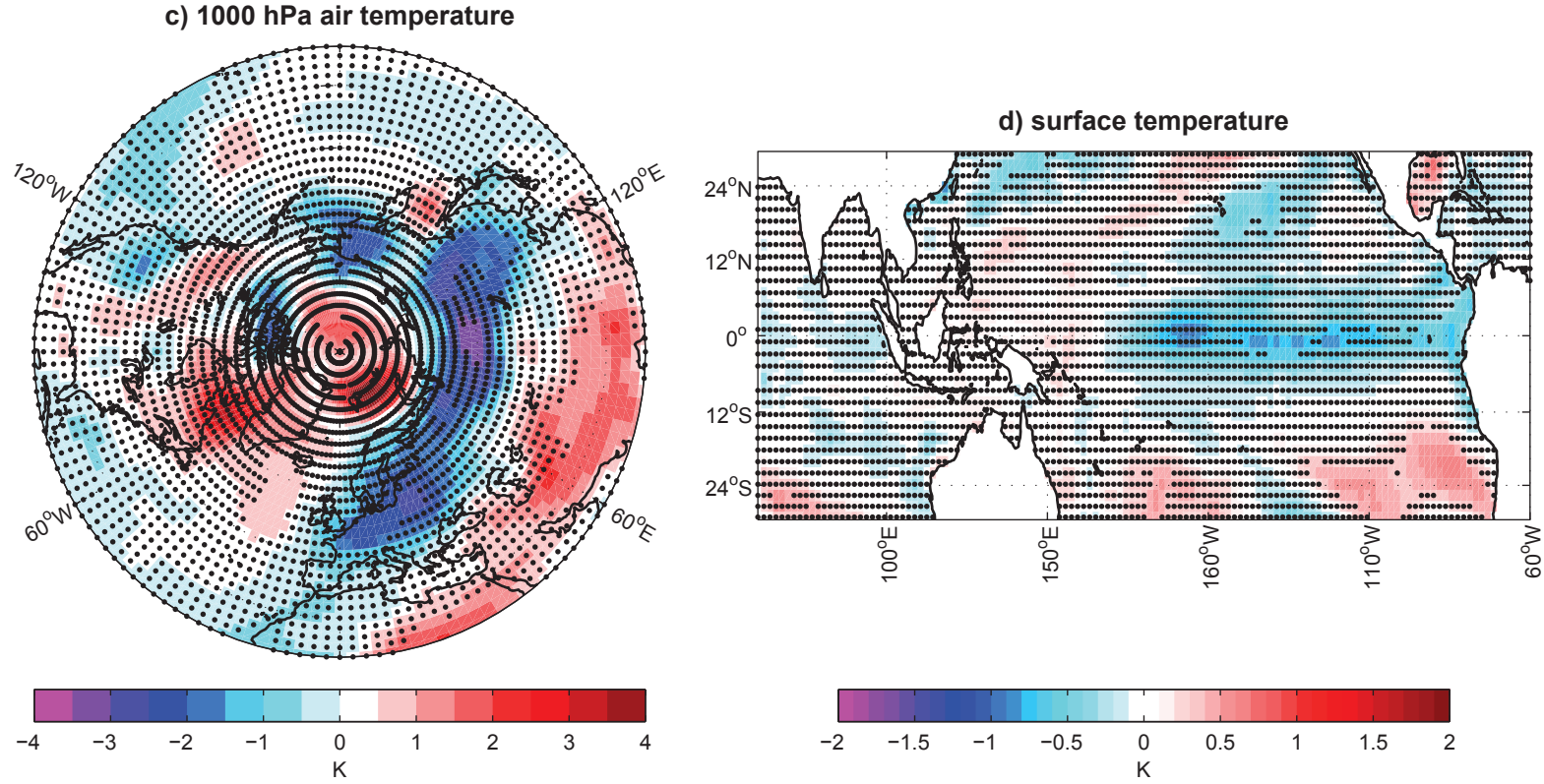
c) 1000 hPa air temperature
120°W
120°E
60°W
60°E
−4 −3 −2 −1 0 1 2 3 4
K
d) surface temperature
24°N
12°N
0°
12°S
24°S
100°E
150°E
160°W
110°W
60°W
−2 −1.5 −1 −0.5 0 0.5 1 1.5 2
K

Figure

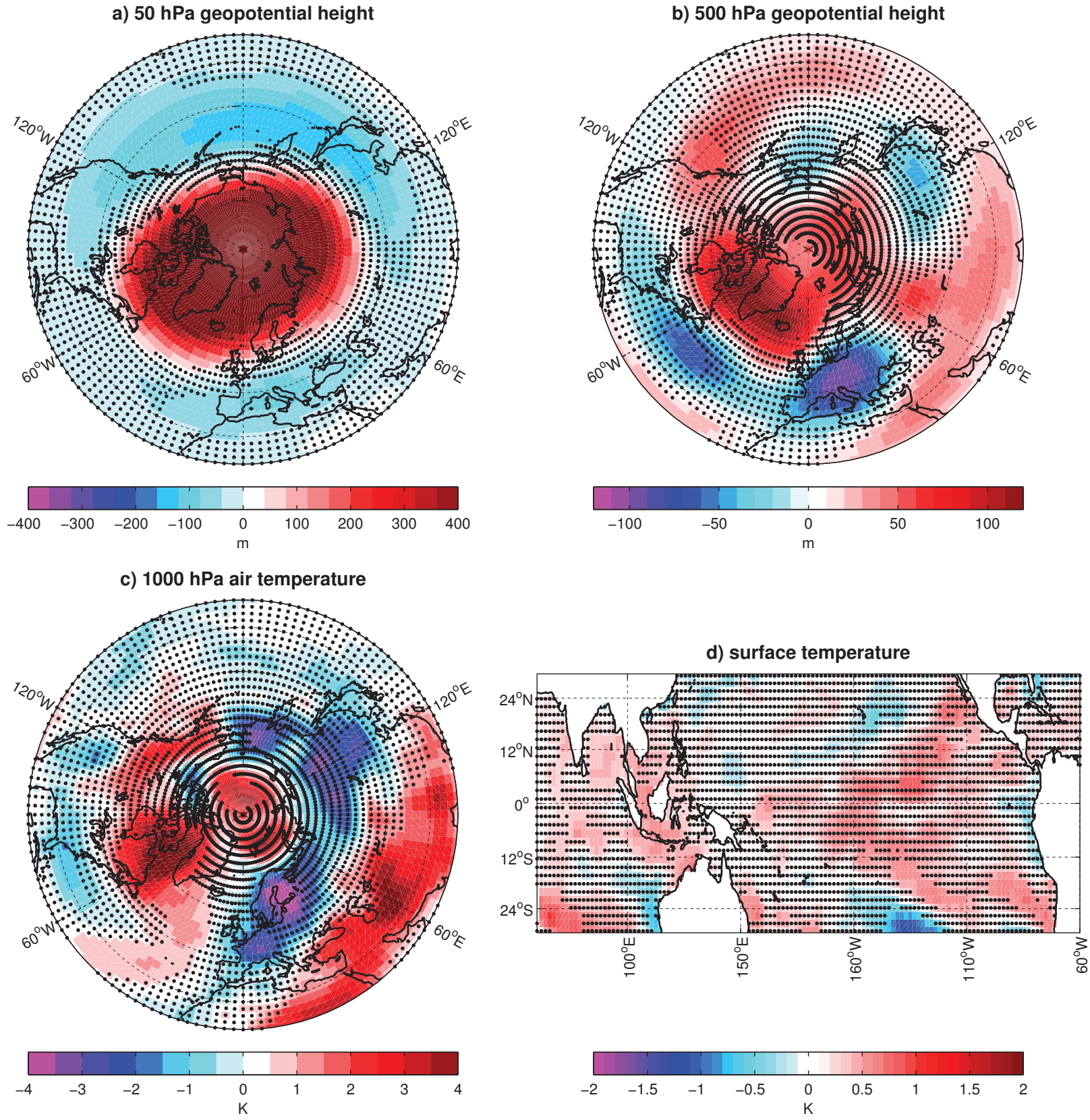
a) 50 hPa geopotential height
120°W
120°E
60°W
60°E
−400 −300 −200 −100 0 100 200 300 400
m
b) 500 hPa geopotential height
120°W
120°E
60°W
60°E
−100 −50 0 50 100
m
c) 1000 hPa air temperature
120°W
120°E
60°W
60°E
−4 −3 −2 −1 0 1 2 3 4
K
d) surface temperature
24°N
12°N
0°
12°S
24°S
100°E
150°E
160°W
110°W
60°W
−2 −1.5 −1 −0.5 0 0.5 1 1.5 2
K

Figure

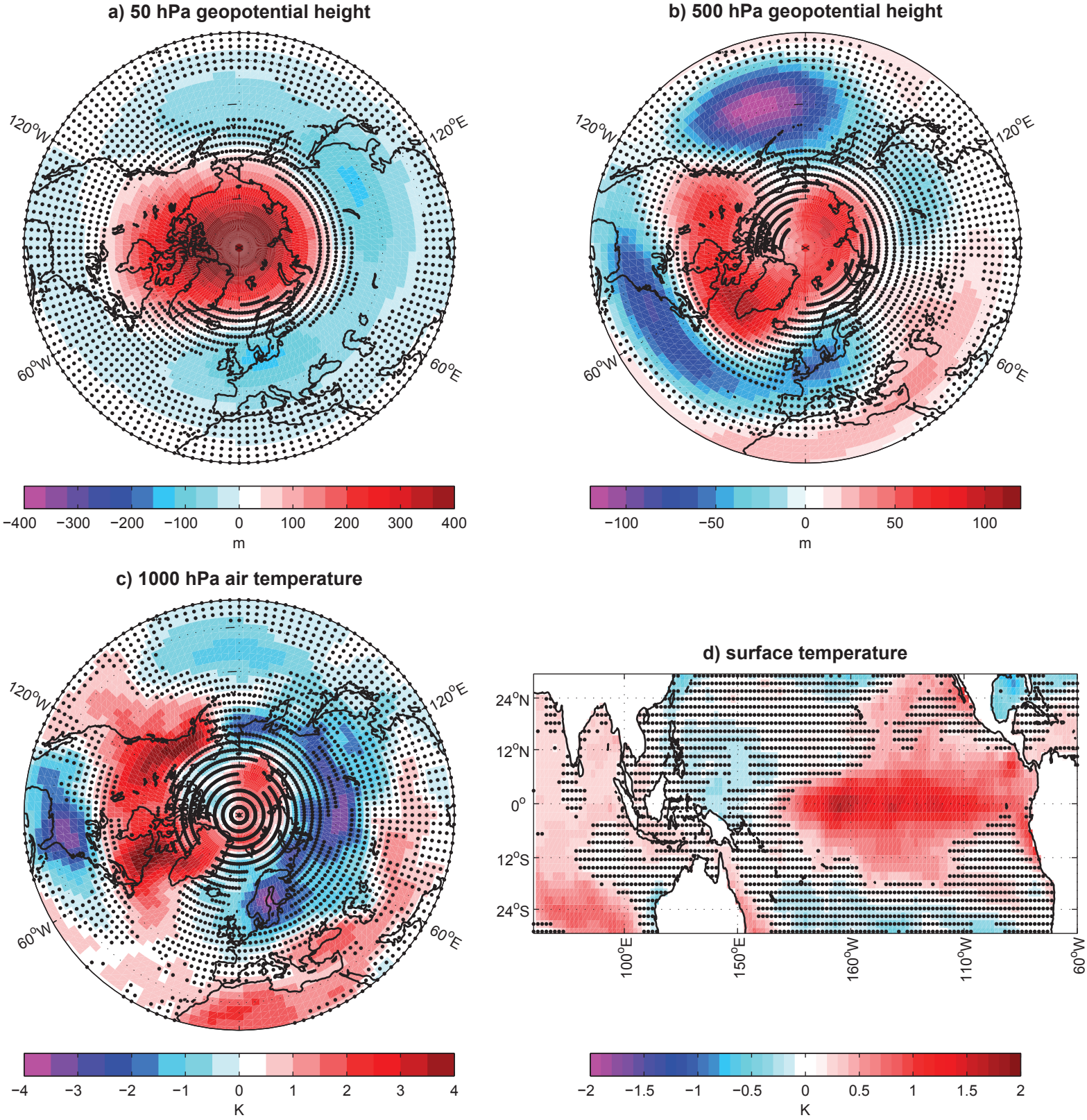
a) 50 hPa geopotential height
120°W
120°E
60°W
60°E
−400 −300 −200 −100 0 100 200 300 400
m
b) 500 hPa geopotential height
120°W
120°E
60°W
60°E
−100 −50 0 50 100
m
c) 1000 hPa air temperature
120°W
120°E
60°W
60°E
−4 −3 −2 −1 0 1 2 3 4
K
d) surface temperature
24°N
12°N
0°
12°S
24°S
100°E
150°E
160°W
110°W
60°W
−2 −1.5 −1 −0.5 0 0.5 1 1.5 2
K

Figure

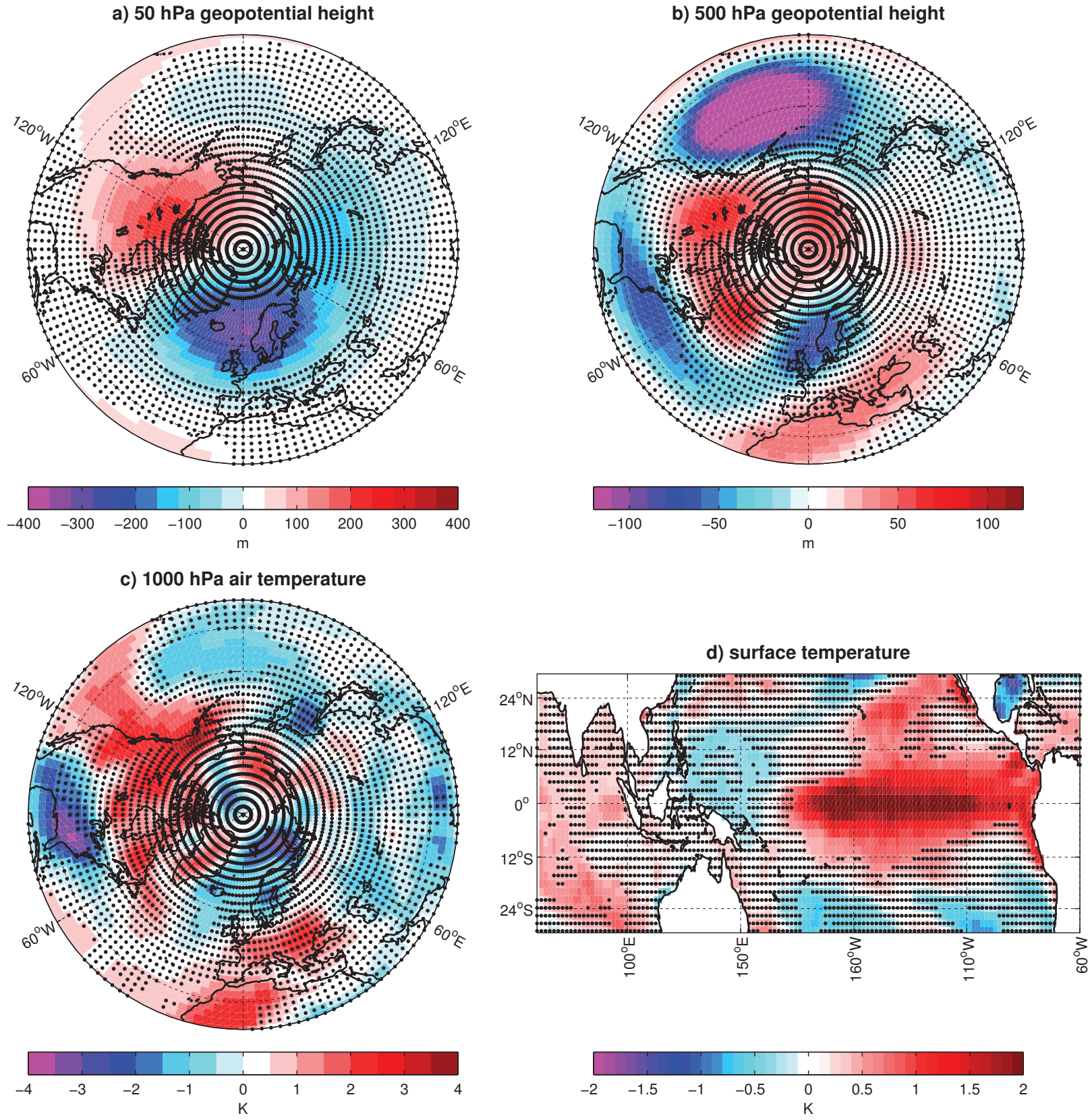
a) 50 hPa geopotential height
120°W
120°E
60°W
60°E
−400 −300 −200 −100 0 100 200 300 400
m
b) 500 hPa geopotential height
120°W
120°E
60°W
60°E
−100 −50 0 50 100
m
c) 1000 hPa air temperature
120°W
120°E
60°W
60°E
−4 −3 −2 −1 0 1 2 3 4
K
d) surface temperature
24°N
12°N
0°
12°S
24°S
100°E
150°E
160°W
110°W
60°W
−2 −1.5 −1 −0.5 0 0.5 1 1.5 2
K

Figure

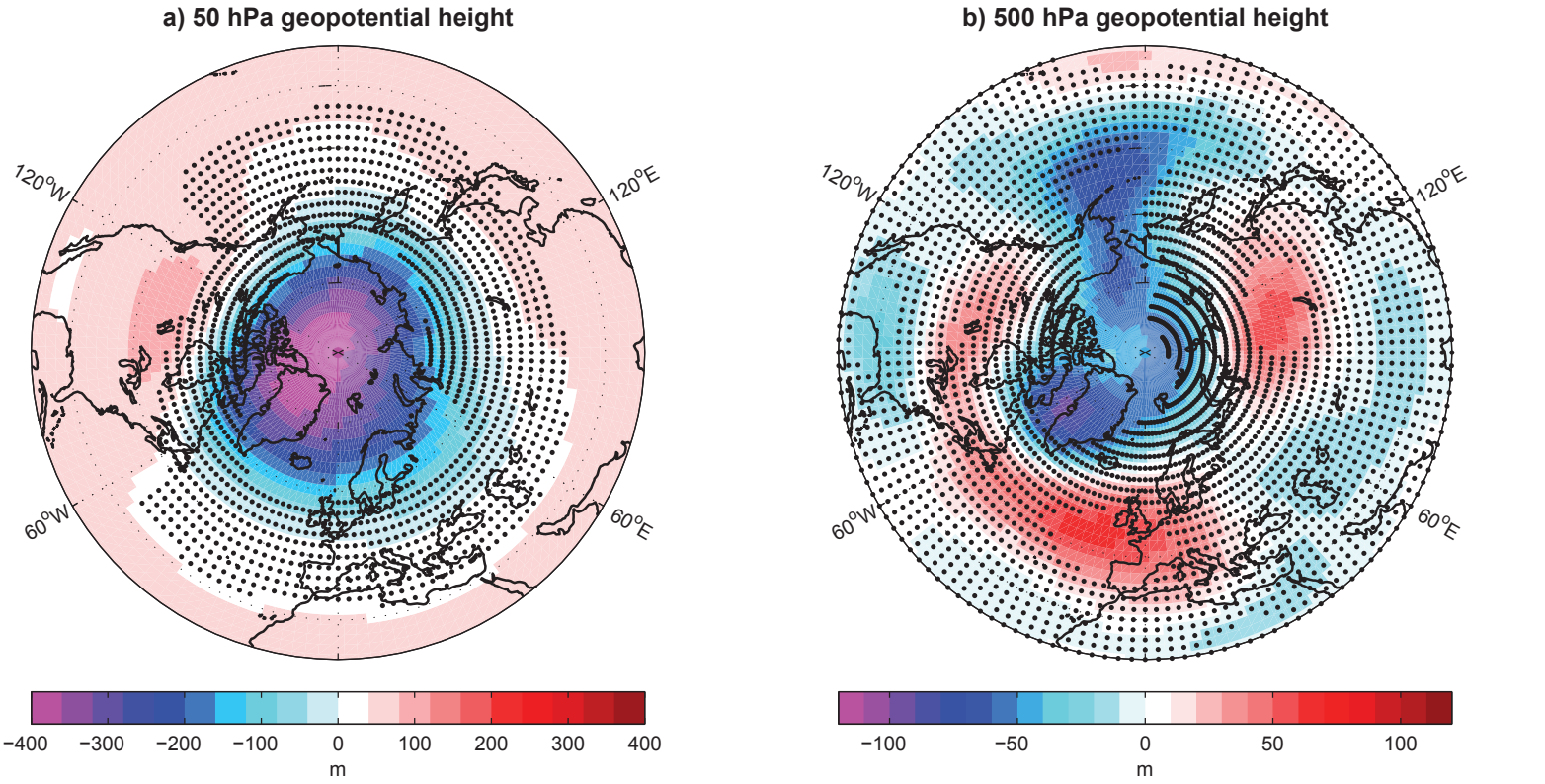
a) 50 hPa geopotential height
120°W
120°E
60°W
60°E
−400 −300 −200 −100 0 100 200 300 400
m
b) 500 hPa geopotential height
120°W
120°E
60°W
60°E
−100 −50 0 50 100
m
c) 1000 hPa air temperature
120°W
120°E
60°W
60°E
−4 −3 −2 −1 0 1 2 3 4
K
d) surface temperature
24°N
12°N
0°
12°S
24°S
100°E
150°E
160°W
110°W
60°W
−2 −1.5 −1 −0.5 0 0.5 1 1.5 2
K

Figure

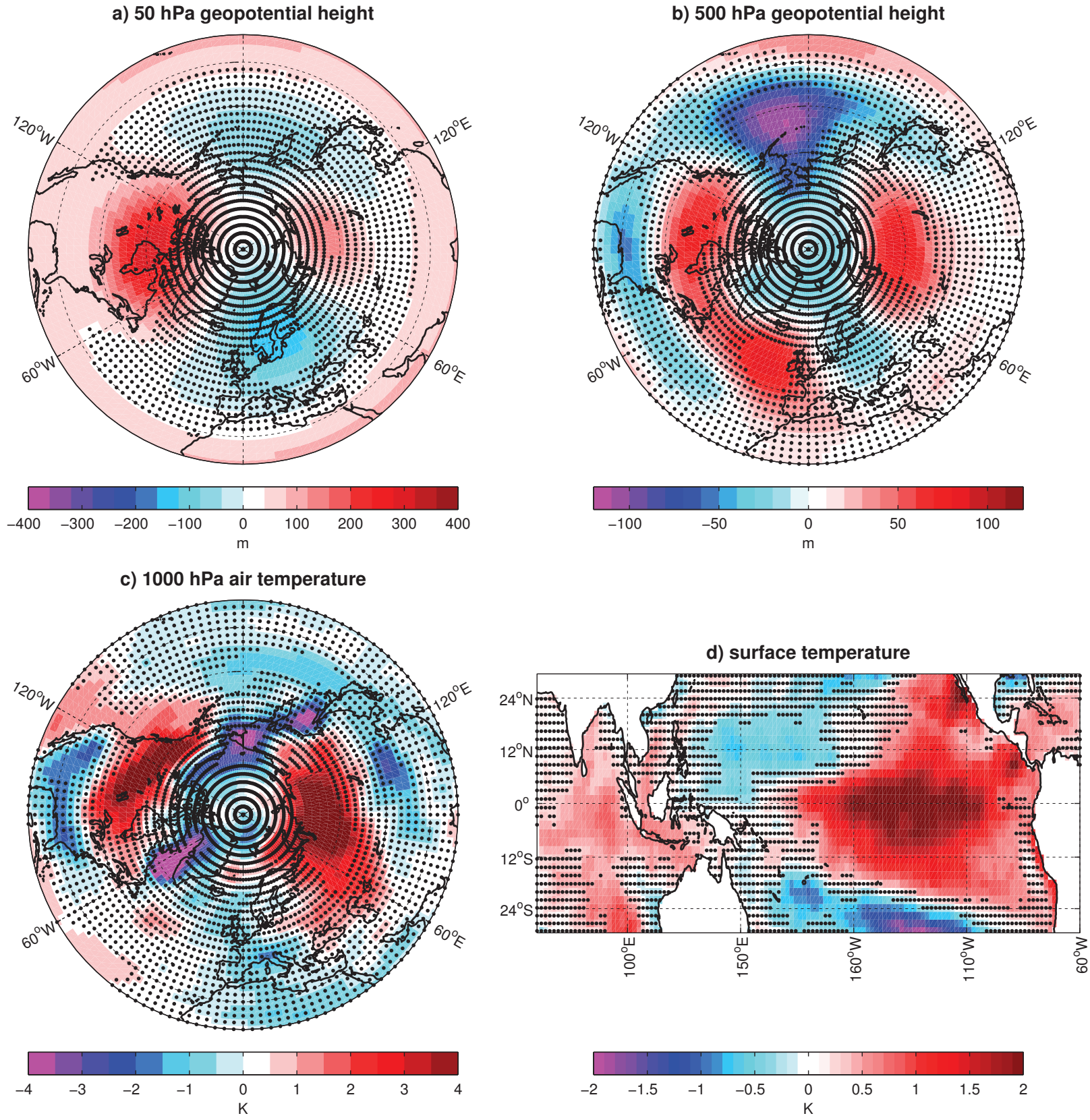
a) 50 hPa geopotential height
120°W
120°E
60°W
60°E
−400 −300 −200 −100 0 100 200 300 400
m
b) 500 hPa geopotential height
120°W
120°E
60°W
60°E
−100 −50 0 50 100
m
c) 1000 hPa air temperature
120°W
120°E
60°W
60°E
−4 −3 −2 −1 0 1 2 3 4
K
d) surface temperature
24°N
12°N
0°
12°S
24°S
100°E
150°E
160°W
110°W
60°W
−2 −1.5 −1 −0.5 0 0.5 1 1.5 2
K

Figure

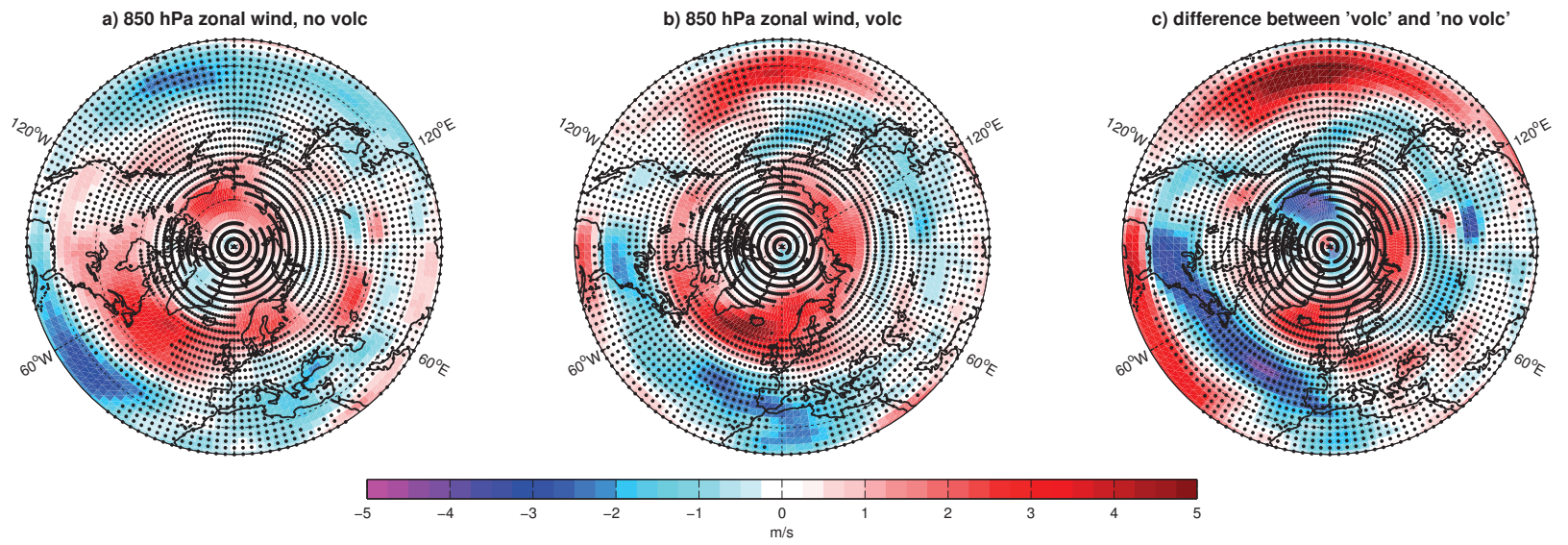
a) 850 hPa zonal wind, no volc
b) 850 hPa zonal wind, volc
c) difference between 'volc' and 'no volc'
120°W
120°E
60°W
60°E
−5
−4
−3
−2
−1
0
1
2
3
4
5
m/s

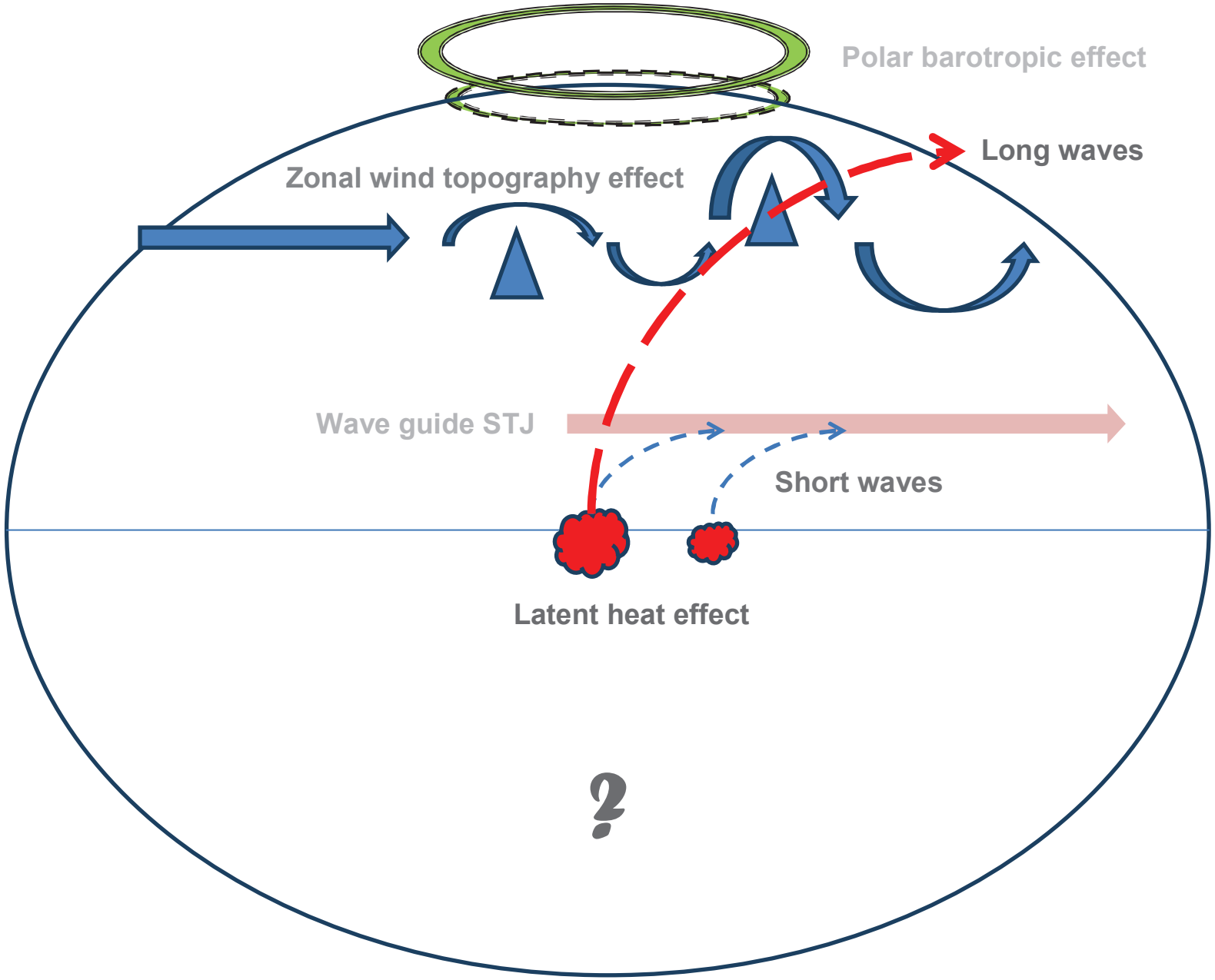
Polar barotropic effect
Long waves
Zonal wind topography effect
Wave guide STJ
Short waves
Latent heat effect
?

Figure